REPORT DOCUMENTATION PAGE

Form Approved
OMB No. 0704-0188

1. REPORT DATE *(DD-MM-YYYY)*	2. REPORT TYPE	3. DATES COVERED *(From - To)*
07-07-2008	Technical Paper & Briefing Charts	

4. TITLE AND SUBTITLE

Preliminary Results of Low Energy Sputter Yields of Boron Nitride due to Xenon Ion Bombardment (Preprint)

5a. CONTRACT NUMBER

5b. GRANT NUMBER

5c. PROGRAM ELEMENT NUMBER

6. AUTHOR(S)
James L. Topper, Binyamin Rubin, Cody C. Farnell, & Azer P. Yalin (Colorado State University)

5d. PROJECT NUMBER

5e. TASK NUMBER

5f. WORK UNIT NUMBER
33SP0853

7. PERFORMING ORGANIZATION NAME(S) AND ADDRESS(ES)

Air Force Research Laboratory (AFMC)
AFRL/RZSS
1 Ara Drive
Edwards AFB CA 93524-7013

8. PERFORMING ORGANIZATION REPORT NUMBER

AFRL-RZ-ED-TP-2008-289

9. SPONSORING / MONITORING AGENCY NAME(S) AND ADDRESS(ES)

Air Force Research Laboratory (AFMC)
AFRL/RZS
5 Pollux Drive
Edwards AFB CA 93524-7048

10. SPONSOR/MONITOR'S ACRONYM(S)

11. SPONSOR/MONITOR'S NUMBER(S)
AFRL-RZ-ED-TP-2008-289

12. DISTRIBUTION / AVAILABILITY STATEMENT

Approved for public release; distribution unlimited (PA #08282A).

13. SUPPLEMENTARY NOTES
For presentation at the 44th AIAA Joint Propulsion Conference, Hartford, CT, 20-23 July 2008.

14. ABSTRACT

We describe the development of an experimental apparatus geared towards measurement of boron nitride sputtering by low energy ions. A four-grid system is used to achieve a collimated beam at low energy (<100 eV). A weight loss approach is used to measure total sputter yields and a quartz crystal microbalance (QCM) is used to measure differential sputter yield profiles of condensable components. Integration of the QCM profiles also gives total sputter yields of condensable components. We report initial results of total and differential sputter yield measurements of three grades of boron nitride due to bombardment by xenon ions with ion energies in the range of 60-250 eV and at ion incidence angles of 0, 15, and 45 degrees from normal. Comparison with past measurement results are made where possible.

15. SUBJECT TERMS

16. SECURITY CLASSIFICATION OF:			17. LIMITATION OF ABSTRACT	18. NUMBER OF PAGES	19a. NAME OF RESPONSIBLE PERSON
					1Lt Michael Gorrilla
a. REPORT	b. ABSTRACT	c. THIS PAGE	SAR	61	19b. TELEPHONE NUMBER *(include area code)*
Unclassified	**Unclassified**	**Unclassified**			N/A

Preliminary Results of Low Energy Sputter Yields of Boron Nitride due to Xenon Ion Bombardment (Preprint)

James L. Topper*, Binyamin Rubin†, Cody C. Farnell‡, Azer P. Yalin§
Colorado State University, Fort Collins, CO, 80523

We describe the development of an experimental apparatus geared towards measurement of boron nitride sputtering by low energy ions. A four-grid system is used to achieve a collimated beam at low energy (<100 eV). A weight loss approach is used to measure total sputter yields and a quartz crystal microbalance (QCM) is used to measure differential sputter yield profiles of condensable components. Integration of the QCM profiles also gives total sputter yields of condensable components. We report initial results of total and differential sputter yield measurements of three grades of boron nitride due to bombardment by xenon ions with ion energies in the range of 60-250 eV and at ion incidence angles of 0, 15, and 45 degrees from normal. Comparison with past measurement results are made where possible.

I. Nomenclature

A_s	=	sensor area of QCM
E	=	beam ion energy
E^*	=	characteristic energy to describe sputtering profile
$J_{B,avg}$	=	time-averaged current of bombarding particles (ions and energetic neutrals)
M_i	=	molar mass of species i
R	=	mass accumulation rate
Y	=	total sputter yield
α	=	polar angle of sputtered particle (from target normal)
β	=	ion incidence angle relative to target normal
Δm	=	mass loss due to ion beam exposure
ϕ	=	azimuthal angle of sputtered particle
ρ	=	density of target material
r_{qcm}	=	distance from the target center to the QCM
y_{MZ}	=	modified Zhang differential sputter yield
y	=	volumetric differential sputter yield

II. Introduction

Ion sputtering is the process in which atoms (and molecules, clusters, or ions) are ejected from the surface of a material due to bombarding incident ions[1]. Details of the sputtering process are of interest from both theoretical and applied viewpoints. Our primary interest is to better understand the role of sputtering in electric propulsion (EP) thrusters used for satellite and space exploration[2-10]. More specifically, we are interested in the sputtering of boron nitride (BN) because of its widespread use as an insulator material in the acceleration channel of stationary plasma

* Graduate Research Associate, Mechanical Engineering, Colorado State University.
† Post-Doctoral Research Associate, Mechanical Engineering, Colorado State University.
‡ Post-Doctoral Research Associate, Mechanical Engineering, Colorado State University.
§ Associate Professor, Mechanical Engineering, Colorado State University, AIAA Member.

thrusters (SPTs). Erosion of the insulator channel is an important thruster life-limiting mechanism, and deposition of the sputtered BN can contaminate spacecraft surfaces (e.g. solar panels or thermal control surfaces).

Owing to relatively long lifetimes (5-10+ years) of EP thruster devices and the complexity and expense of experimental tests, effects of sputter erosion and deposition are generally studied with numeric codes. For erosion studies (lifetime), one aims to compute the amount of surface erosion due to the bombarding ions. The modeling requires knowledge of the total sputter yields (Y) of the eroding materials of interest at the ion conditions of interest. Modeling of deposition additionally requires knowledge of the differential (angular) sputter yields ($y(\alpha,\phi)$) in order to track the trajectories of sputtered particles. Total and differential sputter yield profiles have been measured with a multitude of techniques, a partial list of which includes weight loss[11], collector plates[12-13], mass spectrometry[14], quartz crystal microbalance[3-7,15-16], Rutherford backscattering[17-18], radioactive tracers[19], and cavity ring-down spectroscopy[20].

Despite the importance of BN erosion there is a lack of fundamental sputtering data on BN. In particular, numerical modeling of thruster erosion[21-23] shows that the ions most critical to the erosion process have relatively low energy (<~100 eV). Given the low associated sputter yields, such measurements strain detection limits of many measurement systems, making them especially challenging. The goal of the present submission is to contribute towards filling this gap. In this work we detail development of an experimental configuration for low energy BN sputter measurements. We report initial results for several grades of BN at ion energies down to and below 100 eV. The results presented here represent the start point of a comprehensive study that is currently in progress and encompasses a broader range of sputtering conditions and includes temperature variation studies. The measurement approach is to use a combination of weight-loss and QCM deposition sensor and builds upon our previous work[5-7, 9-10]. In Section III we summarize our experimental apparatus including sputtering chamber, ion source, and weight loss and QCM measurement systems. In Section IV we present sputtering results for bombardment of xenon ions on HBC, HBR, and HP grades of boron nitride including comparison with other measurements (where possible). Finally, conclusions are given in Section V.

III. Experimental

A. Overview of Sputter Measurement System

Sputter measurements are performed using a quartz crystal microbalance (QCM) deposition monitor as well as a weight loss approach. An improvement relative to our past work is that both measurements are performed concurrently in the same facility. The experimental apparatus is shown in Figure 1. The system has been previously described[5-7, 9-10] so that in this subsection we give an overview of its essential features, while the following subsections detail specific aspects and recent modifications. The ion source and QCM are housed within a 0.125 m^3 stainless steel vacuum chamber (43 cm ID x 76 cm long main section), equipped with a 1500 liter/s CTI-8 cryogenic pump. The chamber base pressure was 5×10^{-7} Torr giving a working pressure of approximately 0.6 to 1×10^{-4} Torr. The gridded ion source has been specially designed for low energy operation and is described below in more detail.

A rotatable target-mount is positioned 23 cm downstream of the ion source. Details of the BN targets used are presented in Section IIIC. We have incorporated a heating plate into the sample holder as a means to perform sample bake-outs and to control sample temperature for upcoming temperature dependence studies. The new sample holder is formed from a 6 x 6 x 1 inch plate of stainless steel with four holes drilled into a 6 x 1 inch side. These holes are evenly spaced and each penetrates 4 inches into the plate with a diameter of 0.5 inches. Into each of these holes we place a cylindrical cartridge heater capable of outputting as much as 200 W of power (per cartridge). At full power, the plate can raise the sample temperature as high as 700 °C, although other constraints of the system will limit the temperature to about 500 °C.

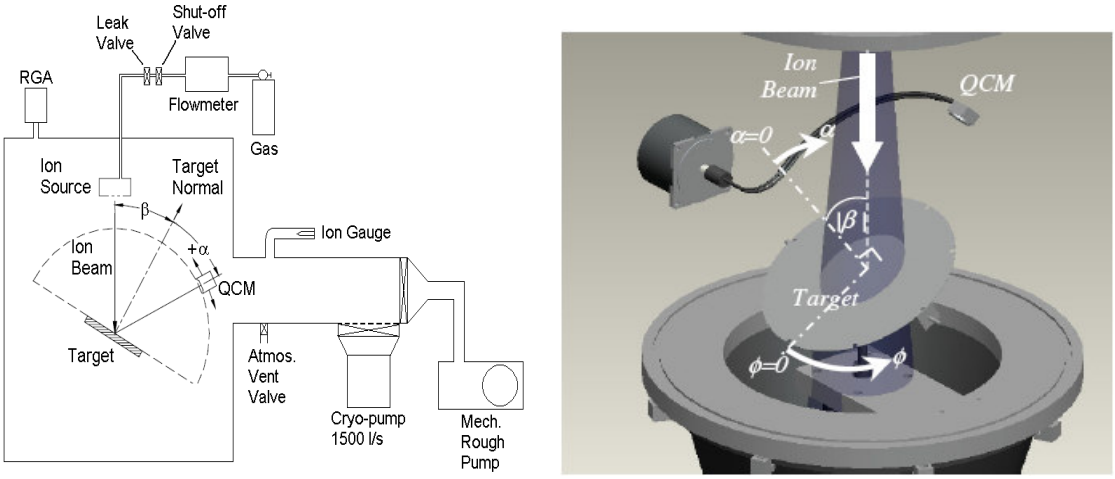

Figure 1. Schematic diagram of experimental set-up

B. Four-Grid Ion Source

We have developed a four-grid ion source to enable collimated beams at the low ion energies of interest to this work. Detail on the design and manufacture of the source will be reported in a future submission. Here, we summarize the operating conditions and ion beam characteristics. The source is designed to operate on xenon gas (typical flow rate of 0.5 sccm) and is based on a plasma discharge chamber operating with a dual filament cathode.

The four-grid ion source consists of a screen grid, an acceleration grid, a focus grid, and a deceleration grid. The screen grid controls the beam energy and is maintained positive to ground, while the acceleration grid draws the ion beam out of the source and is maintained at approximately -600 V relative to ground. The focus grid collimates the beam, and is held negative to ground generally at -125 V. Finally, the deceleration grid helps prevent ion backstreaming, and is generally maintained slightly negative (~2 V) relative to ground. The beam then passes through a ground screen and over a neutralizer filament kept at an emission current of roughly twice the beam current. The filament passes directly through the center of the beam to maximize its efficiency.

Beam profiling tests were performed using a Faraday probe mounted on a multi-axis rotatable base. Profiles were integrated to find total beam current. For typical operating conditions the radius encompassing 90% of the total beam current was ~2 cm. Table 1 shows extracted total beam currents at tested beam energies. We were able to extract high-current and well-collimated beams even at energies as low as 30 eV.

Table 1. Beam energies and currents from four-grid ion source.

Beam Energy (eV)	30	40	60	80	100	150	200	250
Beam Current (mA)	0.97	1.14	1.46	1.96	1.84	2.11	2.94	3.45

During sputter measurements we record (from the power supplies) the ion current leaving the source. Determination of the sputter yield requires the current of energetic particles (ions and fast neutrals) incident on the sputtering target. As in our past work[9,11], we make corrections for charge-exchange and scattering. The charge-exchange beam generates fast neutrals which, depending on scattering angles, may bombard the target. The resulting correction is to multiply the source current by 0.95 ± 0.05.

C. Boron Nitride Targets: Surface Charging and Moisture Effects

Test results reported herein are for HBC, HBR, and HP grades of Boron Nitride (BN). Each of these materials is formed by hot-pressing and corresponds to the graphite-like allotrope of BN. In the base plane, atoms are held together by strongly directed hexagonal arrays of covalent bonds, resulting in impressive electrical, thermal, and mechanical properties. The HBC and HBR materials were obtained from General Electric's (GE's) Advanced Ceramics. Calcium borate is used as binder in HBR, however no binder is used in HBC. The two grades have generally similar properties though with some differences. For example, HBR has higher thermal expansion, higher

moisture absorption, and higher volume resistivity at elevated temperatures. More detail on the materials can be obtained from GE datasheets. The HP grade is obtained from Saint-Gobain and uses calcium borate as a binder.

Our past measurements of insulator materials, including boron nitride, have shown effects of surface charging and the importance of appropriate neutralization. Similar surface charging effects have been observed by Zhang et al.[24] and Nikiporetz et al.[25]. In order to neutralize the surface charge, a plasma bridge neutralizer (PBN) was placed in the chamber close to the sample being sputtered. Details on the neutralization scheme have been presented in our past work[10]. Operating conditions of the PBN include an emission current of 10-15 mA and a Xe mass flow rate of 0.5 sccm. The PBN was biased negatively relative to ground potential, at roughly -15 V.

Our past measurements have shown that HBR BN exhibits effects of moisture absorption and associated mass change at relative humidity levels of less than or equal to 40% at room temperature, while HBC does not[10]. These effects are expected based on moisture absorption information provided in the material datasheets. Similar effects were reported by Garnier[26]. HBR BN can maintain appreciable amounts of moisture even after storage in a dry environment. The exact mechanism of absorption is unclear but it is postulated that the surface undergoes chemical or compositional changes related to the calcium borate binder. Empirically, we find that (for the resolution of our measurements) the mass buildup levels off after approximately one hour after venting the chamber and exposing the targets to the atmosphere. To accommodate this, the approach we follow is to perform the before- and after-measurements in the heavy (moist) state by waiting one hour after removal prior to measuring the mass. The method has been experimentally validated. In our previous work, we have discussed baking the samples for ~0.5 hours to remove absorbed moisture. In the present study, the pre-test bake-out was eliminated. Instead, the samples were heated under the chamber filaments prior to sputtering and only allowed to reach a thermal steady-state condition (~20 minutes). Since the mechanism behind the moisture absorption is not completely understood, it was decided that baking the samples at higher temperature could potentially cause changes in both surface structure of the sample and the chemical composition of the calcium borate binder, which could alter sputter properties.

Similar issues arise for HP BN and limit our ability to do sputter measurements by the weight loss method. The HP BN also contains the calcium borate binder (and in higher mass percentage) so that moisture effects may be expected. In comparison to HBR BN, we found the HP mass to increase at a higher rate and for a longer duration (more than 24 hours). As means of illustration, Fig. 2 shows mass buildup on BN samples after removing from the vacuum chamber. The curves show mass buildup beginning after 90 minutes; mass build-up in the first 90 minutes is at an even higher rate. In summary, it was found that the large mass buildup (and variation of individual samples) relative to the total before/after mass change of a typical test (~2-10 mg) precludes weight loss measurements of HP BN in our current setup. See also discussion of humidity effects in Section IVA. Such effects do not influence QCM measurements so total sputter yields for HP BN can be inferred from QCM results.

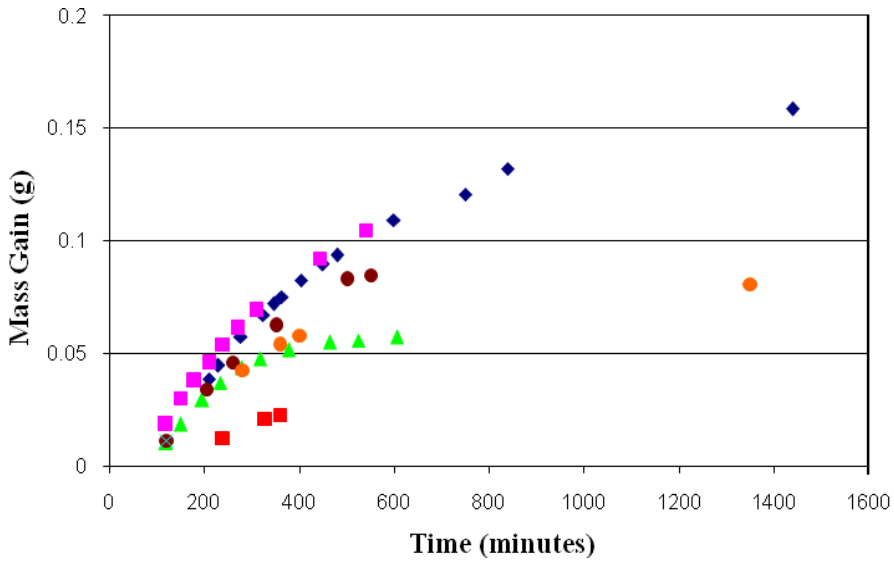

Figure 2. Mass accumulation as a function of time from six different HP BN weighing sessions. Time zero corresponds to 90 minutes after removal from vacuum chamber.

D. Definition of Angles

The angles used to describe the direction of ion incidence and the ejections angles of sputtered particles are shown in Fig. 1. We define as follows: β is the incidence angle of bombarding ions measured relative to the surface normal (β=0 for normal incidence), α is the ejection polar angle of sputtered atoms measured relative to the surface normal, and ϕ is the ejection azimuthal angle of the sputtered atoms measured in the plane of the target surface (defined so that ϕ=0 is in the forward sputter direction i.e. in the forward direction of the plane containing the surface normal and the incident ion directions).

E. QCM Sensor and Signal Analysis

In deposition mode, the QCM allows determination of differential sputter yields through measurement of mass accumulation (of sputtered particles) on its surface. For condensable components, sticking coefficients are assumed to be unity. Note that sticking coefficients for "new layers" and very thin layers (Angstrom thicknesses) may be less than unity, but once a sufficient layer thickness of a given material has accumulated, sticking coefficients for condensables are generally unity[27]. For the BN materials, the sputtered particles may consist of a mix of condensable and noncondensable components; this issue is further addressed in Section IV.

We use a Sigma Instrument SQC-339 Deposition Controller that reads the crystal frequency to 0.001 Hz and an RC-cut quartz crystal as opposed to the more conventional AC-cut crystal. The RC-cut crystal manufactured by Tangidyne Corporation is extremely accurate for deposition of very thin films. Increased sensitivity is achieved by adjusting the stress coefficients of the quartz plate using advanced fabrication methods. For most materials of interest, the RC-cut crystal enables measurement of differential sputter yields at ion energies below 100 eV.

Since quartz crystal resonance frequency is extremely sensitive to temperature variation, it should be maintained at constant temperature during the sputter yield measurements. A PolyScience 9002 Programmable Digital Temperature Controller with circulating bath is used to control the temperature of the QCM. The water is circulating through the stainless steel body of the QCM housing, while the temperature of the water in the bath is controlled to 0.01 °C. As the crystal is moved to different positions during the measurement, the heat flux to it varies due to the change in relative position of the QCM and the heat sources in the system, that is, the ion source and PBN. Therefore although the temperature of the water stays constant, the actual crystal temperature is different at different locations (α angles). A K-type thermocouple wire embedded in a copper holder silver-soldered to the back of the QCM crystal holder is used to monitor QCM temperature, and a LabView program that performs data logging during differential sputter yield measurements has been modified to ensure that the temperature of the QCM is stable during every measurement. When the QCM is moved to the next measurement position, the program monitors its temperature and starts the sputter yield measurements only after the temperature of the crystal has stabilized to within 0.02 °C. The improved temperature stability aids in high signal-to-noise ratio sputter measurements as are needed for low ion energies. The improvement over the previous system is largely due to the direct monitoring of the QCM temperature (as opposed to monitoring of the temperature of water in the circulating bath). The criterion used for temperature stability control can be adjusted if necessary to achieve even higher thermal stability, however each measurement would take substantially longer to acquire.

For a given incidence angle (obtained by tilting the target), the differential sputtering profile is obtained by measuring the sputter yield over two chords above the target: ϕ = 0°/180° and ϕ = 60°/240° (where the latter, by symmetry, also corresponds to ϕ = 120°/300° for azimuthally symmetric sputtering profiles). A total of ~34 positions above the target are typically sampled. At a given measurement point the volumetric differential sputter yield, $y(\alpha,\phi)$, in units of mm^3/C/sr, is determined using equation (1). Note that because we study multi-component materials (for which the sputtered particles may comprise various atoms or molecules), we use volumetric units, e.g. mm^3/C/sr, as opposed to atomic based yields, e.g. atoms/ion. In Eqn. (1), $R(\alpha,\phi)$ is the measured mass accumulation rate (found from a deposition monitor device), ρ is the density of target material, $J_{B,avg}$ (C/s) is the time-averaged current of bombarding particles (ions and energetic neutrals) incident on the target, r_{qcm} is the distance from the target center to the QCM (17.4 cm), and A_s is the QCM sensor area (0.535 cm^2). The quantity A_s/r_{qcm}^2 corresponds to the solid angle that the QCM sensor subtends while $R(\alpha,\phi)/\rho J_{B,avg}$ corresponds to the volume of sputtered material per bombarding charge. Again, it is important to emphasize that the directly measured quantity is the mass buildup of condensable particles on the QCM and the volumetric differential sputter yield should be considered in this way. (In fact the "volume" may not really correspond to any physically observed volume since it corresponds to the

equivalent volume due to the mass of the *deposited condensable material* if one uses the density of the full *target material*; of course conversion to the deposited mass yield simply requires removing the density from Eqn. (1))

$$y(\alpha,\phi) = \left[R(\alpha,\phi) {r_{qcm}}^2 \right] \Big/ \left[\rho J_{B,avg} A_s \right] \tag{1}$$

In principle, because of the finite size of the QCM crystal and beam spot on the target, each of our measurements (i.e. QCM positions) corresponds to a (small) range of polar and azimuthal angles joining the target and QCM. We have performed a simple simulation to show that for our geometry and sputter conditions these effects are negligible (worst case of 5% error), so that we can treat our target and QCM as points (not areas) joined by a single vector[5]. We also note that the viewing angle of the QCM is approximately 5.4 steradians (cone apex angle of 165°) which corresponds to an area on the target that is larger than the irradiated area (also a necessary requirement for equation (1)). Experimental uncertainty and error bars on measured differential sputter yields are found by estimating individual contributions and combining them. Uncertainties are as follows: ± 15% on beam current, ± 6% on radial distance from QCM to target, and ± 0.1% on measurement of the α and ϕ angles. The resultant uncertainty varies depending on measurement conditions but typical uncertainties are approximately ± 16%. For simplicity in analysis, we assume that the uncertainty in total yield Y and E^* from the QCM have the same fractional value.

Analysis and fitting of differential sputter yield profiles requires appropriate functional forms. At our conditions, stopping is predominantly due to elastic (nuclear) collisions and is generally in the linear cascade regime (emitted particles are secondary or higher generation recoils) or single knock-on regime (emitted particles are primary recoils)[1]. A classical theory for the linear cascade regime was originally developed by Sigmund[28]. Independent of ion incidence angle, the original Sigmund theory predicts sputtering profiles that are azimuthally symmetric and approximately diffuse in shape, corresponding to cosine-like profiles of the form $y \propto \cos(\alpha)^n$ (n=1 for a diffuse profile). More recent experimental and numerical studies show a range of profile shapes. For normally incident ions on polycrystalline and amorphous targets, cosine-like profiles are generally observed with increasingly under-cosine shapes as ion energy is lowered and increasingly over-cosine shapes for higher ion energies[5-7,9-10,14,29-31]. For obliquely incident ions at relatively high ion energy, observed profiles also tend to be azimuthally symmetric. However, for lower ion energies the measured profiles tend to be asymmetric with increased sputtering in the forward direction[5-7,9-10,15,19,29]. Similar profiles have been modeled on a theoretical basis[32-34].

As a means to describe the measured differential sputter yield profiles we use expressions from Zhang[35], based on work from Yamamura [33-34], to which we introduce two fit parameters. We term the resulting expressions as Modified Zhang (MZ)[6,14].

$$y_{MZ} = \frac{Y}{1-\sqrt{\frac{E^*}{E}}\cos(\beta)} \cdot \frac{\cos(\alpha)}{\pi} \left[1 - \frac{1}{4}\sqrt{\frac{E^*}{E}} \left(\cos(\beta)\gamma(\alpha) + \frac{3}{2}\pi \sin(\beta)\sin(\alpha)\cos(\phi) \right) \right] \tag{2a}$$

$$\gamma(\alpha) = \frac{3\sin(\alpha)^2 - 1}{\sin(\alpha)^2} + \frac{\cos(\alpha)^2 \left(3\sin(\alpha)^2 + 1\right)}{2\sin(\alpha)^3} \ln\left(\frac{1+\sin(\alpha)}{1-\sin(\alpha)} \right) \tag{2b}$$

where y_{MZ} is the differential sputter yield, Y is the total sputter yield, E is the ion energy, E^* is a characteristic energy describing the profile shape, and the angles are as defined above. The approach decouples the amplitude of the angular profiles from their shape, through the use of Y and E^* respectively. More recent work by Zhang et al[28] also discusses the use of a varying energy parameter, but in the context of expressions for energy distributions and total sputter yields. In general, rather than using the MZ expressions for *a priori* calculation, we treat Y and E^* as free fit-parameters which we determine from (least-squares fitting) experimental data. Note that profile shapes are determined by the ratio E^*/E and for high ion energy ($E^*/E \ll 1$) the MZ expression reduces to the diffuse yield ($y = Y\cos(\alpha)/\pi$).

F. Weight Loss Analysis

A microgram scale was used to weigh the samples (before and after each sputtering session). With this method the volumetric sputter yield, Y (in units of mm^3/C), of each sample is found using Eqn. (3), where Δm represents the mass loss due to ion beam exposure, t is the exposure time, and other symbols are defined as above:

$$Y = \frac{\Delta m}{\rho \, J_{B,Avg} \, t} \tag{3}$$

Measurement uncertainties for total sputter yields were calculated by estimating individual contributions and combining them. Uncertainties are as follows: ± 15% on beam current, ± 200 μg on mass measurements, and ±1% on test time lengths. The error on mass tends to dominate at low yields, and we comment that the quoted mass uncertainty is an order of magnitude larger than that provided by the scales themselves. The resultant uncertainty varies depending on measurement conditions but typical uncertainties are approximately 25%. Note that this value is a random error resulting from finite accuracy of the mass, current, and time measurements. The influences of other factors affecting the accuracy, such as humidity variation, are not taken into account in this calculation. See a discussion of possible factors affecting the accuracy of the weight loss measurements in Section IVA.

G. Measurement Procedure

Targets are deliberately pre-sputtered to better represent the conditions found in long-duration EP operating applications. Pre-sputtering for HBC and HBR targets is an inherent consequence of reusing the same targets used in our past sputter tests. Prior to initial testing, the (new) HP BN target was pre-sputtered to clean its surface and remove any potential surface layers. Pre-sputtering was accomplished by a 750 eV ion beam with a current density of ~1 mA/cm² for 2 hours. An order-of-magnitude estimate for the typical dose of incident ions on a target prior to testing is approximately $10^{20\text{-}21}$ ions/cm^2 (corresponding to 10s-100s of hours and eroded thickness of approximately 10-100 microns). Target contamination effects are estimated to be negligible, since for typical conditions the flux of ions incident on the target is approximately 10 times higher than the flux of nitrogen (the major contaminant) to the target[7].

Before placement into the vacuum chamber, targets are placed on the scales described above. Each target is weighed several times to ensure stability, and the average value of the measured masses is taken. Targets are then inserted into the vacuum chamber and the sputter measurement is conducted. Test durations are fixed such that the mass change of the test is large compared to the precision of mass measurements, and such that the QCM has time (at each position) to sufficiently stabilize relative to thermal and background noise. Test times vary from several hours for the higher energy tests (250 eV) to as long as 14 hours for the lower energy tests (60 eV). After each test, the targets are again weighed and the difference in masses is used for the weight-loss measurement. As described in Section IIIC, we do not perform weight loss measurements for the HP samples, and special considerations are employed for the HBR samples.

IV. Results & Discussion

A. Total Sputter Yields

Validation of our total sputter yield measurements was performed by using molybdenum as a control. While there is variation in data from different research groups, molybdenum sputter yields are reasonably well characterized[36]. We have measured the total sputter yield of Mo at normal incidence at energies of 80, 150, and 200 eV. The total yields from weight loss and QCM (found from the Y parameter of the best-fit MZ profile) were self-consistent and in agreement with the Yamamura and Tawara curve fit[36] to within experimental uncertainty (see Section IIIE). These agreements are taken as validation of the measurement methods and in particular of the assumption that the sticking coefficient of the QCM may be taken as unity for condensables. Figure 3 shows total sputter yields measured by weight loss as a function of ion energy for HBC grade and HBR grade boron nitride for normal incidence.

It should be mentioned that the measurements of total sputter yield values were performed multiple times for the majority of the data points. The reproducibility of the QCM results was good, while the weight loss based sputter yield values varied significantly. For the cases when several measurements were done at the same conditions, the

average value is reported. Random measurement errors, discussed in section IIIF, cannot explain these variations, so the error bars on the weight loss sputter yield plots are based on the reproducibility of the measurements, rather than on the values described in section IIIF. The mass error is attributed primarily to effects of humidity and moisture absorption. The work is ongoing to understand moisture pickup effects and to modify the measurement procedure in order to minimize their influence.

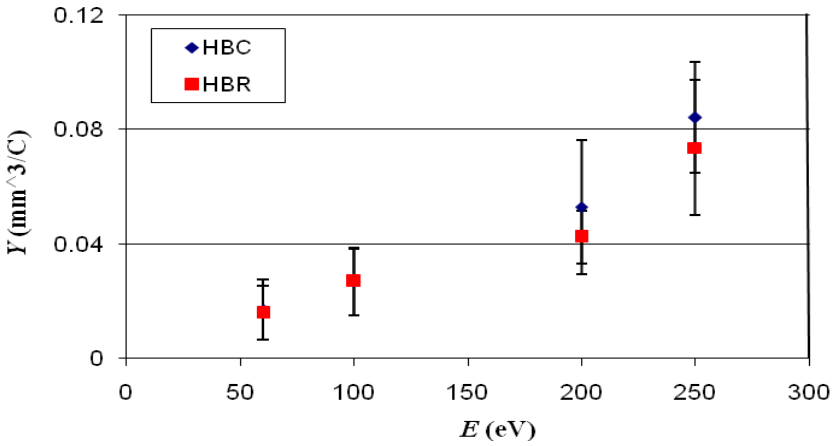

Figure 3. Total sputter yield from weight loss versus ion energy for normal incidence. 100 eV data points coincide.

Using the *Y* parameter of the best-fit MZ profile (equivalent to integrating the best-fit profile) we also obtain total sputter yield results from the QCM measurements. Total yields found in this way, for normal incidence ions, are plotted in Fig. 4. Recall that the QCM measures only condensable components that stick to the QCM, which for BN corresponds to atomic boron and B_xN_y clusters (including BN), but not nitrogen. Therefore, one expects total yields from QCM measurement to be below the weight loss values. (Note that the QCM measurement would actually be more useful in certain cases, such as for modeling of deposition and sticking of sputtered particles to spacecraft surfaces.) Following these ideas, Fig. 5 plots the ratio of total yield from weight loss to the corresponding yield from QCM measurements. We find that the ratio of the weight loss to QCM yields tends to be >1.75 which corresponds to BN sputter products being predominantly atoms. If all sputtering was as B_xN_y clusters, the ratio of yields would be unity, while if all sputtering was as atomic boron and nitrogen the ratio would be 2.30 (= $(M_B+M_N)/M_B$, where M_B and M_N are atomic masses of B and N respectively). Sputtering as atoms is consistent with past mass spectrometry results[1] and multi-component sputtering theory suggests sputtering predominantly as atoms.

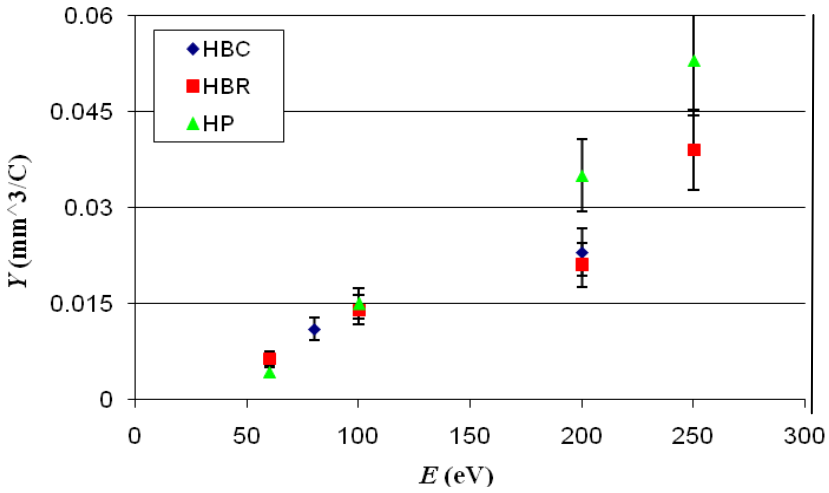

Figure 4. Total sputter yield from QCM versus ion energy for normal incidence.

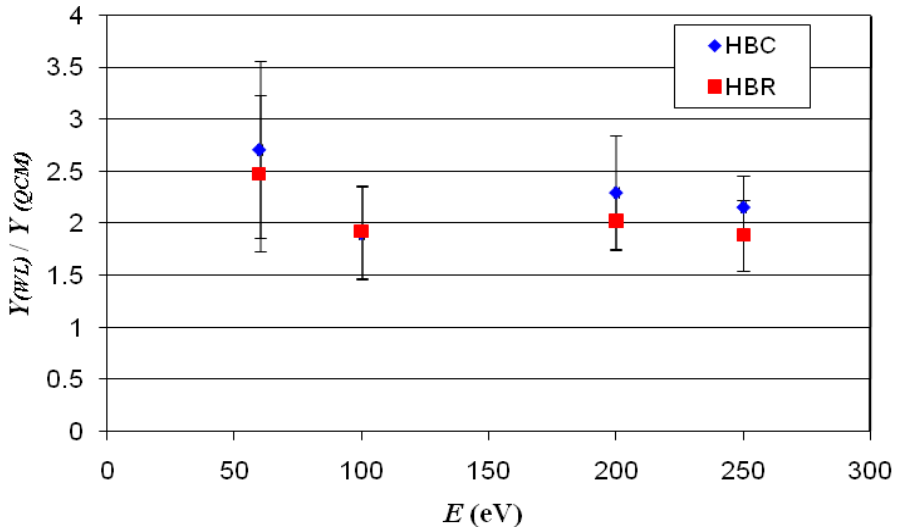

Figure 5. Total sputter yield from weight loss divided by total sputter yield from QCM (see text).

We have studied the variation of total sputter yield with incidence angle at a fixed energy of 100 eV. Measurements have been performed with both weight loss and QCM and results are shown in Fig. 6 and Fig. 7 respectively. The weight loss results are higher than QCM results for the reasons described in connection with Fig. 5. For the QCM data the trend is for the yields to somewhat increase over the range of angles measured consistent with past research[37]. The increase with angle is rather weak for weight loss measurements. This is contrary to the QCM data, to our past measurements and to other published data, where total sputter yield increases with the incidence angle. The reasons of this discrepancy are not clear and will require further investigation. One possible explanation is that due to the graphite-like structure of hot-pressed BN, the probability of xenon ion implantation, i.e. of xenon ion becoming stuck between the molecular planes of BN, increases with incidence angle. Xenon ion implantation has been observed in the past during sputter yield measurements of ceramic materials[38]. If the number of xenon atoms stuck in the target increases with the incidence angle, then while the actual sputter yield also increases, the superposition of the two trends can result in almost flat measured sputter yield vs. incidence angle dependence. Note that the QCM measurements should not be affected be xenon implantation, which is in agreement with the data presented on Fig.7, where total sputter yield increases with the increase of incidence angle.

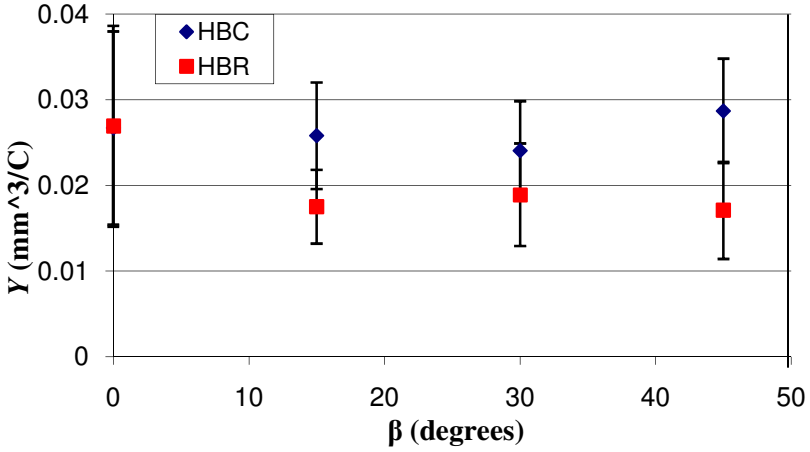

Figure 6. Total sputter yield from weight loss versus incidence angle for 100 eV ion energy.

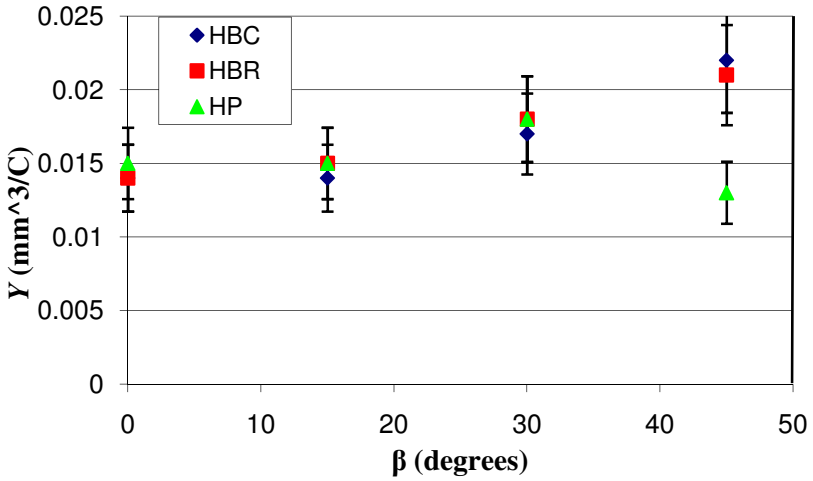

Figure 7. Total sputter yield from QCM versus incidence angle for 100 eV ion energy.

Where possible, we compare our measured HBC BN (weight loss) total sputter yields with measurements and modeled values from other research groups. Figure 8 shows our recent measurements along with weight loss measurements by Semenov[39], Garnier [26], Abashkin[40], and Yim[21]. Note that not all of the authors specify the grade of BN used. We note that the values we are currently reporting are somewhat higher relative to past measurements. Ongoing work is examining possible systematic errors including humidity effects mentioned above.

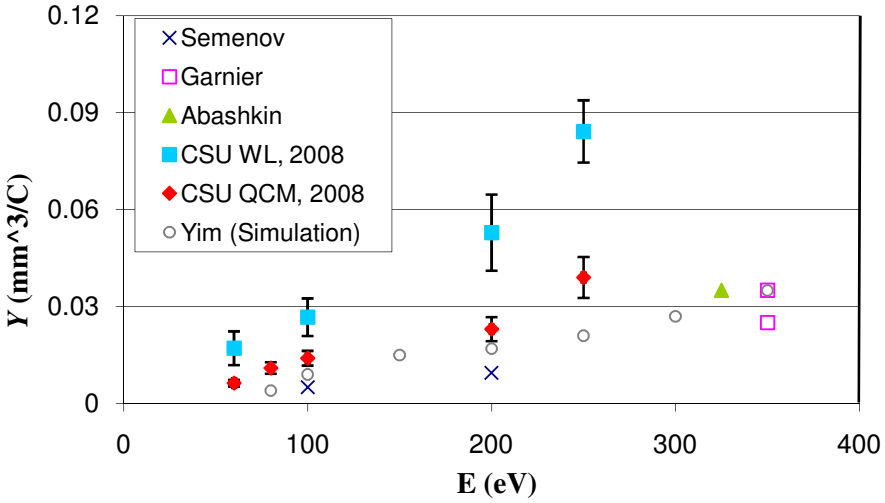

Figure 8. Total BN sputter yields as compared with published values.

We also discuss our total yield measurements in comparison to past measurements from our laboratory[9-11]. We find that the currently reported total yields from the QCM are generally within error of the previously reported values. However, the currently reported weight loss values are higher by a factor of 2-3 relative to previously reported values. The reasons for this discrepancy are unclear; however, we do comment that in the past, the QCM and weight loss measurements have been performed in different chambers and not concurrently. Further, the past weight loss measurements used different neutralization schemes. The improvements in experimental configuration and consistency of data suggest that that the current results should be considered to be more accurate. On the other hand, as discussed above, the values appear elevated to those in the literature and are therefore being more closely examined.

B. Differential Sputter Yields

Using the QCM measurement technique we have measured differential sputter yield profiles. As described in Section IIIE, the MZ expressions are used to fit the profile shapes and the parameter *E*/E* describes the *shape* of the profile. Figure 9 shows the variation in *E*/E* for normal incidence as a function of ion energy for the three grades of BN. Figure 10 shows the variation in *E*/E* at 100 eV as a function of incidence angle for the three grades of BN.

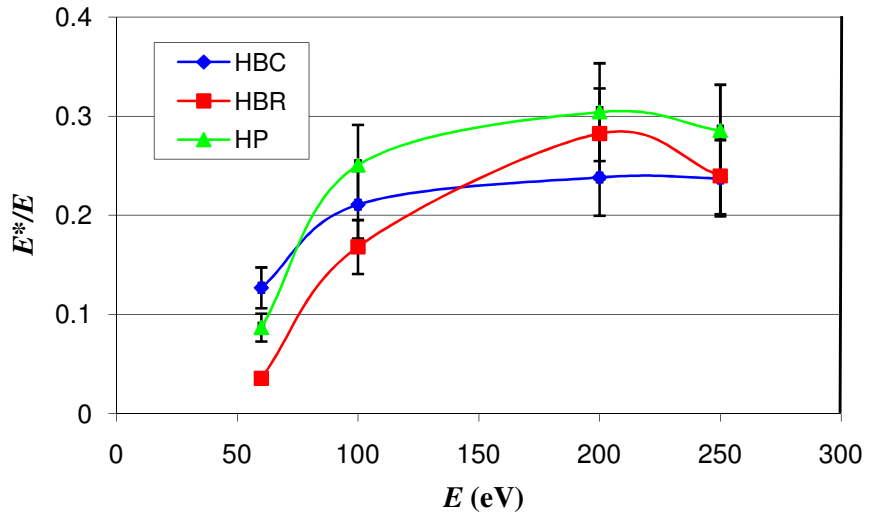

Figure 9. *E*/E* versus ion energy for normal incidence.

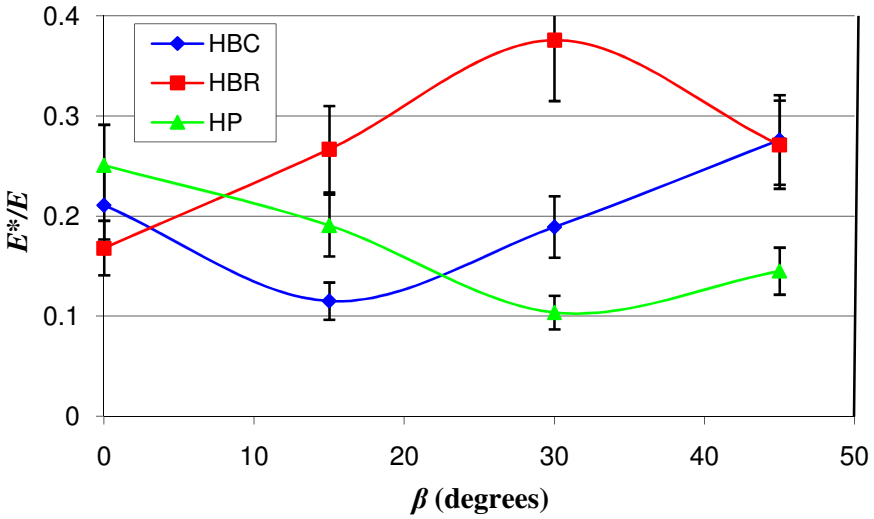

Figure 10. *E*/E* versus incidence angle for 100 eV ion energy.

Examples of comparison between measured (raw) QCM data and fitted MZ profiles are given in Fig. 11. Both plots are for xenon ion energies of 100 eV on HBC BN, with the left plot being at normal incidence and the right plot being at 30 degrees incidence. The plots include QCM measured points, best-fit MZ profiles, and (for comparison) diffuse profiles with the same total yield. One can see relatively good agreement between the measured profiles and MZ profiles. The normally incident profile is azimuthally symmetric. The profile for 30 degrees incidence is measured in the forward/backward plane (ϕ=0,180 degrees) and shows a forward sputter lobe (negative alpha) and reduced sputtering in the backward direction (positive alpha). In general, the MZ expressions provide reasonable descriptions of the measured profiles, but tend to predict a slightly broader and lower amplitude forward-sputter lobe.

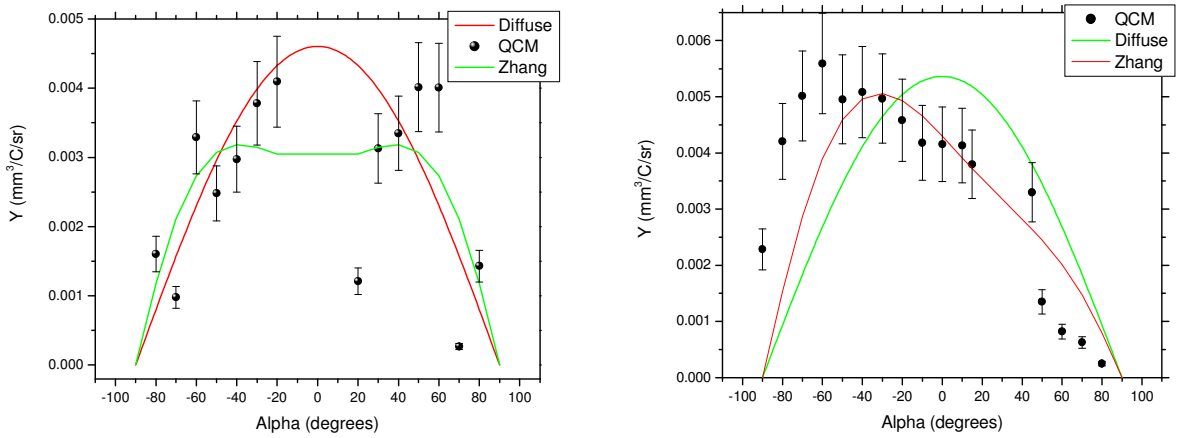

Figure 11. Example of QCM data with best-fit MZ profiles for 100 eV ions on HBC BN. Left: Normal incidence. Right: 30 degrees incidence.

In Fig. 12 we plot examples of the best-fit MZ differential sputter yields using colored hemispheres. Colors (indicated in legend) correspond to the yield in the given direction. For normal incidence the profile is azimuthally symmetric, while for increasingly non-normal incidence the profiles show increasing forward sputter lobes. Interestingly, even for 15 degrees incidence, the profile is already significantly azimuthally asymmetric. Our past work has measured differential sputter yield profiles for some of the same conditions[10]. The shapes measured here are similar to those of the past work with *E*/E* ratios consistent to approximately +/- 0.2. This degree of consistency corresponds to qualitatively similar shapes in our current versus past measurements

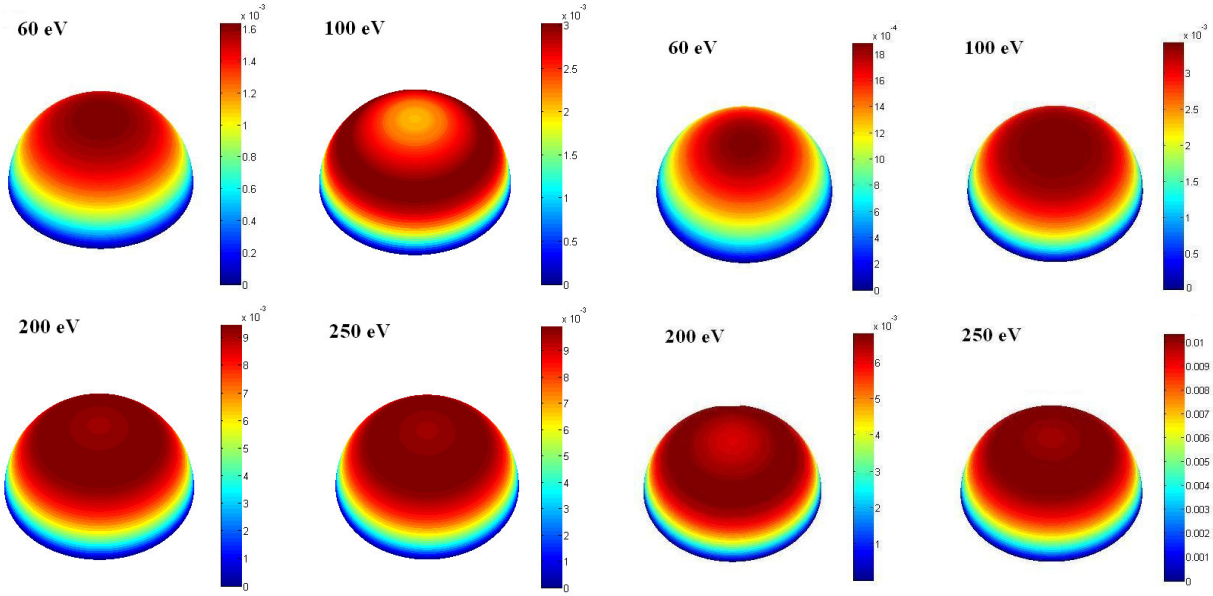

Figure 12. Differential sputter yield profiles for normal incidence at different beam energies. Left: HBC-grade BN. Right: HBR-grade BN

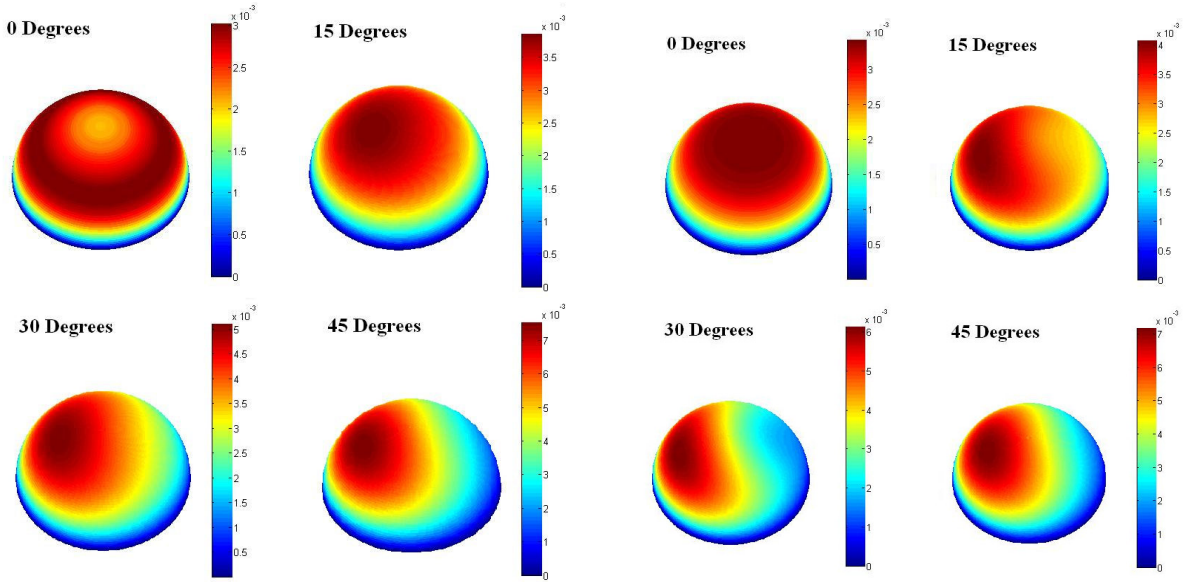

Figure 13. Differential sputter yield profiles for 100 eV ion energy at varying incidence angle. Left: HBC-grade BN. Right: HBR-grade BN.

V. Conclusions

We have detailed the development of an experimental apparatus targeted at low energy sputter yield measurements. We have reported total and differential sputter yield measurements for three grades of BN: HBC, HBR, and HP. Measurements have been performed using a weight loss approach (for total sputter yield) and a QCM measurement approach for differential sputter yield profiles and total sputter yield of condensable components. Using a novel four-grid source we have performed the first, to our knowledge, measurements of BN sputtering in the 100 eV range and below. Effects of humidity (moisture pickup) and xenon ion implantation are possibly affecting the accuracy of our measurements and ongoing work seeks to mitigate these effects. The experimental error on our current measurements is rather large and limits our ability to compare with published results. We do observe higher yields relative to published data and the reasons for this are under ongoing investigation. In comparison to a representative refractory metal such as molybdenum, we find comparable volumetric yields for BN, though the corresponding BN mass- (or atomic-) based yields are still ~5x lower due to the lower density of BN.

Angular dependence of sputtering has been studied using the QCM measurement apparatus and we find that the MZ profiles provide a reasonable description of the measured profiles. The shapes (E^*/E values) for the three grades of BN are all relatively similar and show azimuthally symmetric behavior at normal incidence and forward/backward sputtering features at oblique incidence. Comparison of total yield results from the QCM and weight loss measurement systems give information on the composition of sputtered particles, since the former method captures only condensable particles. We find that the total yields from weight loss are roughly twice those of the QCM, indicating that sputtering is largely as atoms (with boron atoms captured by the QCM, but not nitrogen atoms). This information is particularly relevant for interpretation of future laser diagnostics systems based on CRDS which will measure only boron contributions[41].

There is a critical need in the EP community for low ion energy sputter measurements of BN, and the present contribution is a step forward filling this gap. The results presented here are part of a comprehensive study currently underway. Upcoming and ongoing work aims to measure the BN sputtering over a broader range of sputtering conditions and includes study of variation of sputter yields with BN temperature.

Acknowledgments

The authors would like to thank Air Force Research Labs (Edwards Air Force Base, CA) for funding support. The authors also thank Paul Wilbur (Colorado State University) for initial development of the QCM apparatus, John Williams (Colorado State University) for assistance with the QCM apparatus and ion source, and Casey Farnell (Colorado State University) for additional assistance with the ion beam profiling equipment.

References

[1]Betz G and Wien K 1994 Energy and angular distributions of sputtered particles International *J.Mass Spectrometry and Ion Processes* 140 1-110

[2]Tartz M, Neumann H, Fritsche B, Leiter H, and Esch J 2004 Investigation of sputter behaviour of ion thruster grid materials 40th Joint Propulsion Conference AIAA Paper 2004-4114

[3]Kolasinski R D 2005 Oblique angle sputtering yield measurements for ion thruster grid materials 41st Joint Propulsion Conference AIAA paper 2005-3526

[4]Kolasinksi R D, Polk J E, Goebel D and Johnson L J 2006 Carbon sputtering yield measurements at grazing incidence 42nd AIAA/ASME/SAE/ASEE Joint Propulsion Conference (Sacramento, CA) AIAA 2006-4337

[5]Zoerb K A, Williams J D, Williams D D and Yalin A P 2005 Differential sputtering yields of refractory metals by xenon, krypton, and argon ion bombardment at normal and oblique incidences 29th International Electric Propulsion Conference (Princeton, NJ) IEPC-2005-293

[6]Yalin A P, Williams J D, Surla V, Wolf J and Zoerb K A 2006 Azimuthal differential sputter yields of molybdenum by low energy ion bombardment *42nd AIAA/ASME/SAE/ASEE Joint Propulsion Conference* (Sacramento, CA)

[7]Yalin A P, Williams J D, Surla V, and Zoerb K A 2007 Differential Sputter Yield Profiles of Molybdenum due to Bombardment by Low Energy Xenon Ions at Normal and Oblique Incidence" *Journal of Physics D – Applied Physics* 40 3194-3202

[8]Polk J E 1999 An overview of the results from an 8200 hour wear test of the NSTAR ion thruster paper 35th Joint Propulsion Conference AIAA Paper 99-2446

[9]Yalin, A., Rubin, B., Domingue, S., Glueckert, Z., and Williams, J., "Differential Sputter Yields of Boron Nitride, Quartz, and Kapton Due to Low Energy Xe^+ Bombardment" *43rd AIAA/ASME/SAE/ASEE Joint Propulsion Conference* (Cincinnati, OH)

[10]Rubin, B., Topper, J., and Yalin, A., "Total and Differential Sputter Yields of Boron Nitride Measured by Quartz Crystal Microbalance and Weight Loss," *30th International Electric Propulsion Conference* (Florence, Italy) IEPC-2007-074

[11]Yalin A P, Surla V, Farnell C, Butweiller M, and Williams J D 2006 Sputtering Studies of Multi-Component Materials by Weight Loss and Cavity Ring-Down Spectroscopy, 42nd AIAA Joint Propulsion Conference (Sacramento, CA)

[12]Chiplonkar V T and Rane S R 1965 Dependence of angular distribution of sputtering by positive ions from metal targets on the impact angle Indian J. Pure Appl Phys 3 161

[13]Tsuge H and Esho S 1981 Angular distribution of sputtered atoms from polycrystalline metal targets J. Appl. Phys. 52 4391-95

[14]Wucher A and Reuter W 1988 Angular distribution of sputtered particles from metals and alloys J. Vac. Sci. Tech. A 6 (4) 2316-18

[15]Mannami M, Kimura K and Kyoshima A 1981 Angular distribution measurements of sputtered Au atoms with quartz oscillator microbalances Nuclear Instruments and Methods 185 533-37

[16]Wickersham C E and Zhang Z 2005 Measurement of angular emission trajectories for magetron-sputtered tantalum Jnl. Electronic Materials 34

[17]Shutthanandan V, Ray P, Shivaparan N, Smith R, Thevuthasan T and Mantenieks M 1997 On the measurement of low-energy sputtering yield using rutherford backscattering spectrometry 25th International Electric Propulsion Conference (Cleveland, OH) IEPC-97-069

[18]Mantenieks M, Foster J, Ray P, Shutthanandan S, and Thevuthasan T 2001 Low energy xenon ion sputtering yield measurements 27th International Electric Propulsion Conference (Pasadena, CA) IEPC-01-309

[19]Kundu S, Ghose D, Basu D, Karmohapatro S B 1985 The angular distribution of sputtered silver atoms Nuclear Instruments and Methods in Physics Research B 12 352-57

[20]Surla V and Yalin A P 2007 Differential sputter yield measurements using cavity ring-down Applied Optics, 44, 30, pp. 6496-6505

[21]Yim, J., "Computational Modeling of Hall Thruster Channel Wall Erosion," Ph.D. Dissertation, Dept. of Aerospace Engineering, University of Michigan, MI, 2008

[22]Cheng, S., "Computational Modeling of a Hall Thruster Plasma Plume in a Vacuum Tank," MS Thesis, Dept. of Aeronautics and Astronautics, Massachusetts Inst. of Tech., MA, 2002

[23]Ustarroz, J., Caro, I., Corengia, P., Garmendia, I., Marcos, J., Ahedo, E., and Gonzales del Amo, J., "Specific laboratory testing equipment & methodology for sputtering tests of electric propulsion materials," *30th International Electric Propulsion Conference* (Florence, Italy) IEPC-2007-167

[24]Zhang L and Zhang L Z 2005 Anisotropic energy distribution of sputtered atoms induced by low energy heavy ion distribution Rad. Effects & Defects in Solids 160 337-47

[25]Nikiporetz, E., Semenov, A., Shkarban, I., Khartova, E., "Sputtering process of BN based ceramic by the flows of noncompensated charge plasma," *30th International Electric Propulsion Conference* (Florence, Italy) IEPC-2007-7
[26]Garnier Y et al. 1999 Low-energy xenon ion sputtering of ceramics investigated for stationary plasma thrusters J. Vac. Sci. Tech. A 17 (6) pp. 3246-3254
[27]Bachmann, L., and Shin, J.J., "Measurement of the Sticking Coefficients of Silver and Gold in an Ultrahigh Vacuum," *J. Appl. Phys.*, Vol. 37, No. 1, 1966, pp. 242-246.
[28]Sigmund P 1969 Theory of sputtering I: sputtering yield of amorphous and polycrystalline targets Phys. Rev. 184 383-416
[29]Wehner G K and Rosenberg D 1960 Angular distribution of sputtered material J. App. Phys. 31 177-9
[30]Chini T K Tanemura M and Okuyama F 1996 Angular distribution of sputtered Ge atoms by low keV Ar+ and Ne+ ion bombardment Nucl. Instr. and Methods in Physics Research B 119 387-91
[31]Yamamura Y and Muraoka K 1989 Over-cosine angular distributions of sputtered atoms at normal incidence Nucl. Instr. and Methods in Physics Research B 42 175-81
[32]Yamamura Y 1981 Contribution of anisotropic velocity distribution of recoil atoms to sputtering yields and angular distributions of sputtered atoms Rad. Eff. 55 49–55
[33]Yamamura Y 1982 Theory of sputtering and comparison to experimental data Nucl. Instr. and Meth. 194 515–22
[34]Zhang Z L and Zhang L 2004 Anisotropic angular distributions of sputtered atoms Radiation Effects and Defects in Solids 159 301-07
[35]Zhang J. et al. 1997 Sputtering investigation of boron nitride with secondary ion and secondary neutral mass spectrometry J. Vac. Sci. Tech. A 15 (2) 243-247
[36]Yamamura, Y., and Tawara, H., "Energy Dependence of Ion-Induced Sputtering Yields from Monatomic Solids at Normal Incidence," *At. Data Nucl. Data Tables*, Vol 62, No. 2, 1996, pp. 149-253.
[37]Yamamura, Y., Itikawa, Y., and Itoh, N., "Angular Dependence of Sputtering Yields of Monatomic Solids," *Institute for Plasma Physics Report* IPPJ AM-26, 1983
[38]Khartov, S., personal communication, September 2007
[39]Semenov A., Shkarban, I., "Ion Beam Sputtering of the Surfaces of Ion and Plasma Sources," *Rocket and Space Engineering: Rocket Engines and Power Plants,* No.3, 1991, pp.42-53 (in Russian).
[40]Abashkin, V., Gorshkov, O., Lovtsov, A., and Shagaida, A., "Analysis of Ceramic Erosion Characteristic in Hall-Effect Thruster with Higher Specific Impulse," *30th International Electric Propulsion Conference* (Florence, Italy) IEPC-2007-133
[41]Yalin, A., Tao, L., Yamamoto, N., Smith, T., and Gallimore, A., "Boron Nitride Sputter Erosion Measurements by Cavity Ring-Down Spectroscopy," *30th International Electric Propulsion Conference* (Florence, Italy) IEPC-2007-075

Preliminary Results of Low Energy Sputter Yields of Boron Nitride due to Xenon Ion Bombardment

James Topper, Binyamin Rubin,

Cody Farnell, Azer Yalin

Department of Mechanical Engineering

Colorado State University

44th AIAA/ASME/SAE/ASEE Joint Propulsion Conference, Hartford, CT, July 23, 2008

Outline

- Background
- Experimental
  - Sputter Facility
  - Weight Loss
  - Quartz Crystal Microbalance (QCM)
- BN Materials
- Total Sputter Yield Measurements
- Differential Sputter Yield Measurements
- Conclusions

Sputtering Process

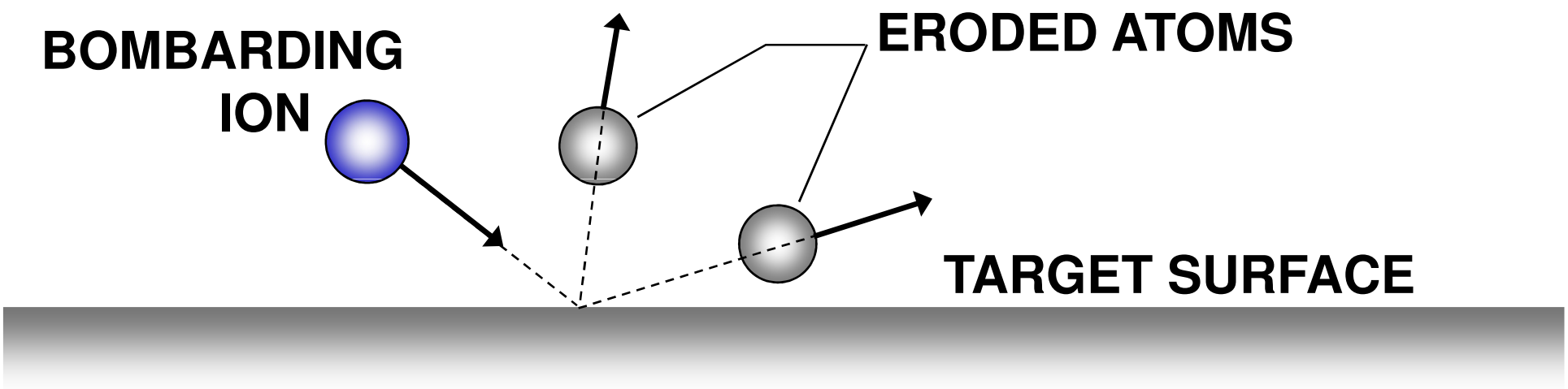

Sputter Erosion Measurements

- Sputtering is key mechanism that places ***fundamental limitations on ion and plasma thruster life times***
- Sputtered material can cause ***space craft contamination***

→ Device measurements and material characterization measurements needed for code validation/development

- Available Techniques: Weight loss, deposition monitor, surface layer activation, profilometry, LIF, optical emission, CRDS

BN Erosion in SPTs

- Erosion of BN insulator leads to end of life in stationary plasma thrusters (SPTs).
- Low energies (~<100 eV range) critical.

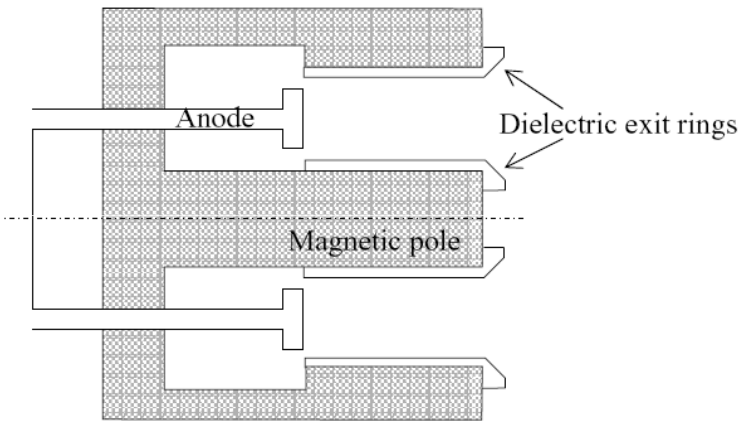

S.Y. Cheng et al.,IEPC-2007-250

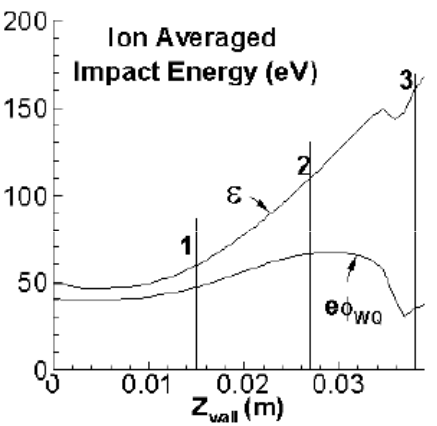

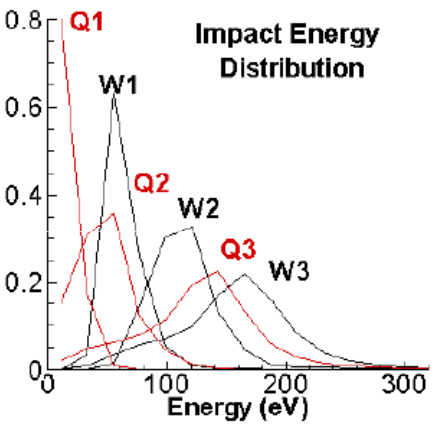

E. Ahedo et al.,IEPC-2007-067

Recent Papers:

•E. Ahedo et al., Simulation of wall erosion in Hall thrusters , IEPC-2007-067

•S.Y. Cheng et al., Modeling of Hall thruster lifetime and erosion mechanisms, IEPC-2007-250

•R. Hofer et al., BPT-4000 Hall Thruster Discharge Chamber Erosion Model Comparison with Qualification Life Test Data, IEPC-2007-267

•J.T. Yim et al. Hydrodynamic Modeling of Krypton and Xenon Propellant Performance in a Hall Thruster, AIAA 2007-5210

Total and Differential Sputter Yields

- Total yield:

Y (atoms/ion → mm^3/C)

$Y = Y(E, \beta, \text{material (grade)}, T)$

where: E = ion energy, β = incidence angle, T = temperature

- Differential yield:

Y (atoms/ion/sr → mm^3/C/sr)

$Y = \text{Y} \times y'(\alpha, \phi)$

where: α = polar ejection angle, ϕ = azimuthal ejection angle

$$Y \equiv \int y(\alpha,\phi)d\Omega = \int_0^{2\pi}\int_0^{\pi/2} y(\alpha,\phi)\sin(\alpha)d\alpha d\phi$$

- Diffuse: $y = \frac{Y}{\pi}\cos(\alpha)$
- Or: $y \propto \cos^n(\alpha)$

Available BN Sputter Data

Limited data available, especially at low energy (<~100 eV)

- Effect of grades?
- Temperature?
- Incidence angle?
- ….

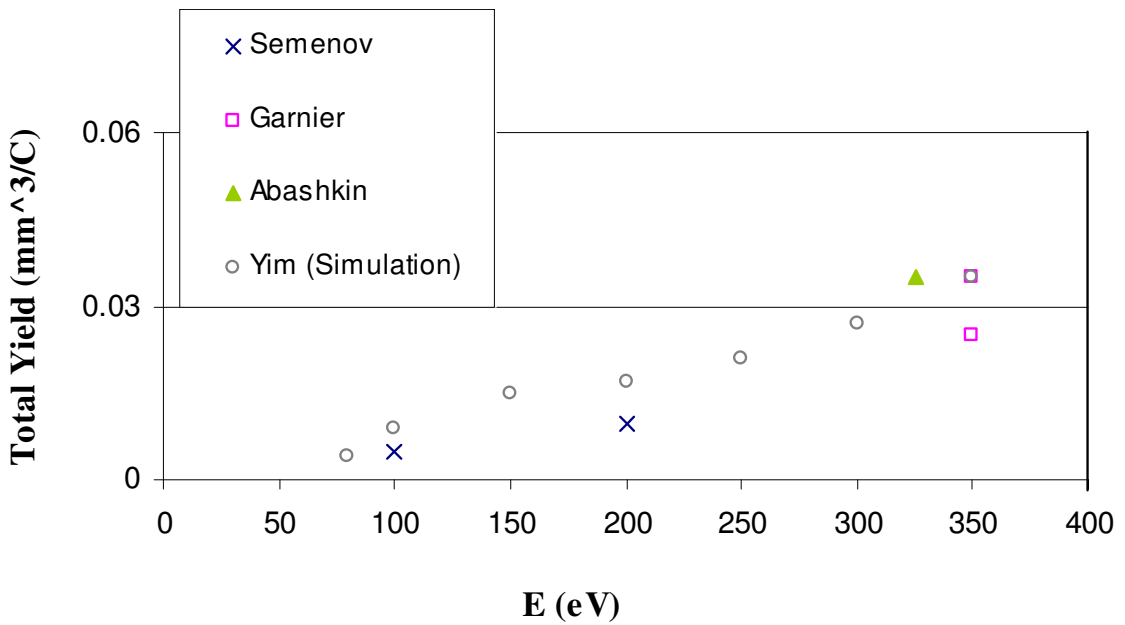

Sputter Measurement Apparatus

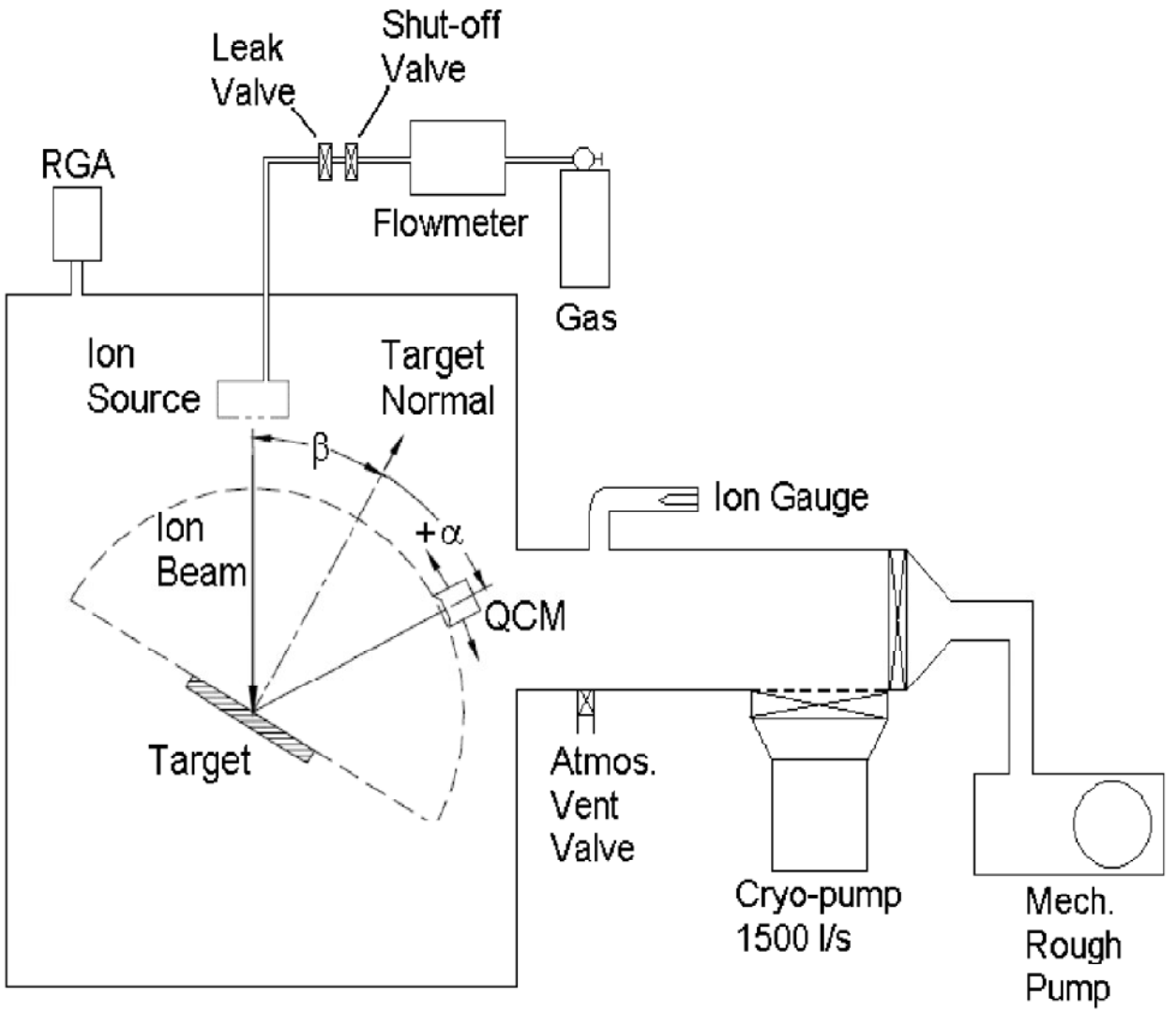

Sputter Measurement Apparatus

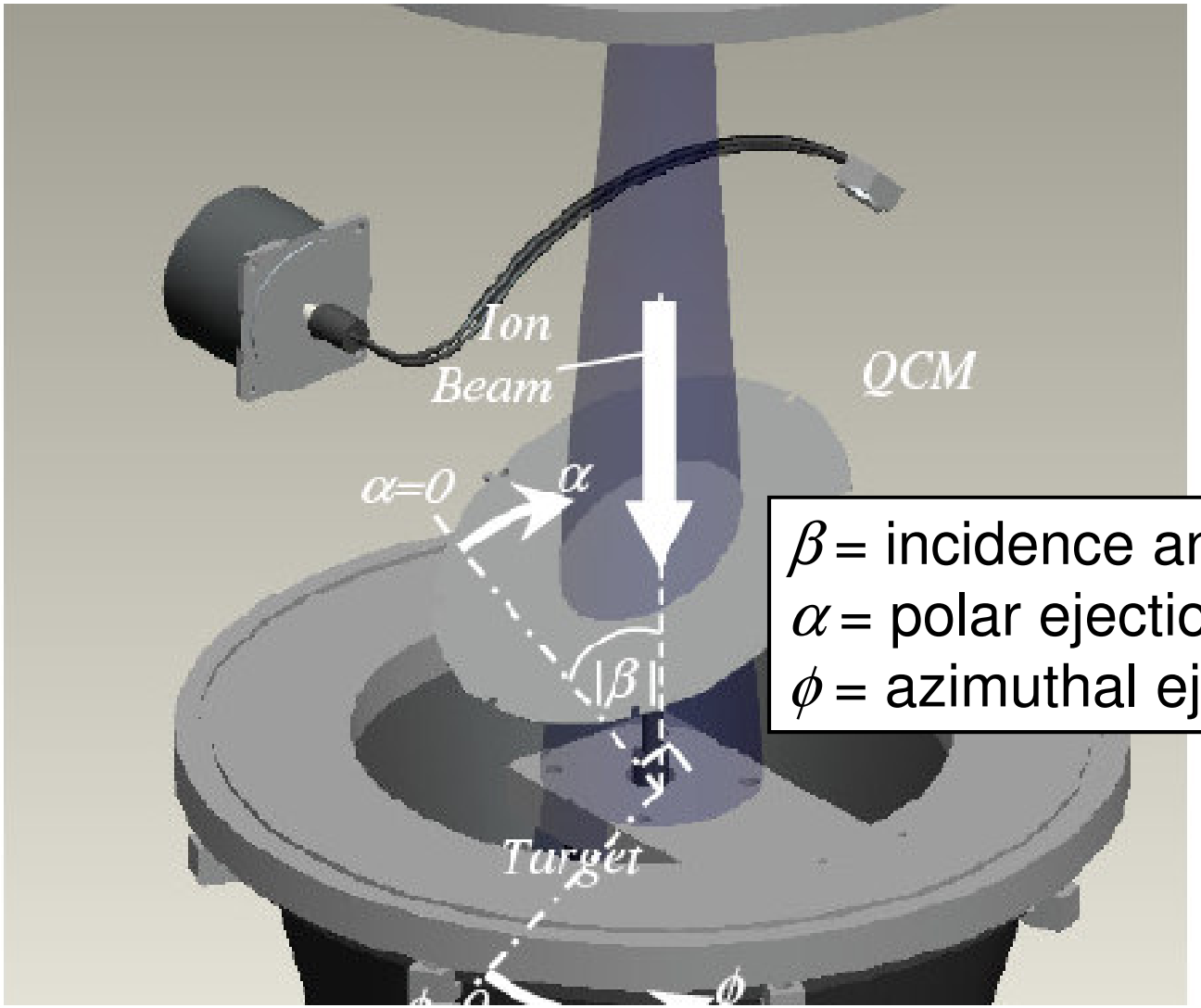

β = incidence angle
α = polar ejection angle
ϕ = azimuthal ejection angle

Sputter Measurement Apparatus

- Stainless steel vacuum chamber 0.125 m^3. Baseline pressure below $1*10^{-6}$ Torr
- CTI-8 cryogenic pump (1500 liter/s for air)
- Hot filament ion source (four grid ion optics system)

- Neutralizers: filament – ion beam neutralization, and PBN – sample surface neutralization
- Sigma Instruments SQC-339 deposition controller (reads the crystal frequency to 0.001 Hz)
- RC-cut QCM (Tangydine corp.)
- Polyscience 9000 series digital temperature controller that allows temperature control to better than 0.01 K
- Compumotor motion control system
- LabView based data acquisition system

Four-Grid Ion Source – make slide

- Our old (two-grid system) was limited by ~100 eV
- A new four-grid ion optics enables to extract collimated beams at the low ion energies (below 100 eV)
- We were able to extract well-collimated beams
- even at energies as low as 30 eV

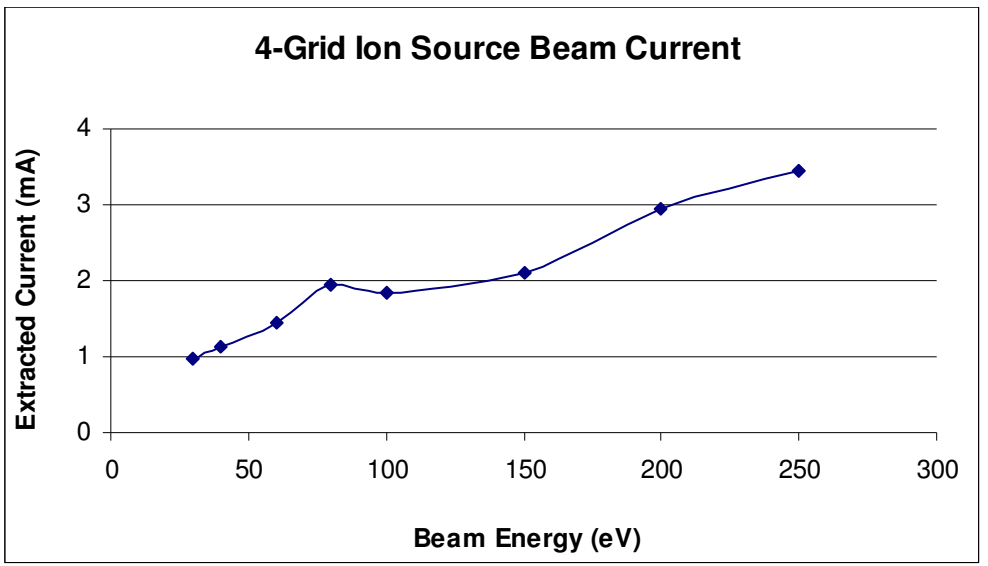

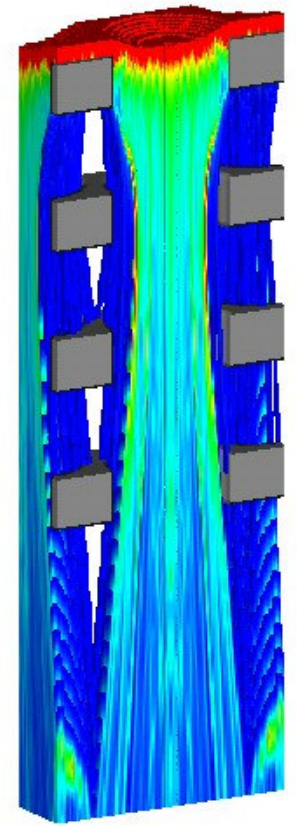

QCM Deposition Monitor

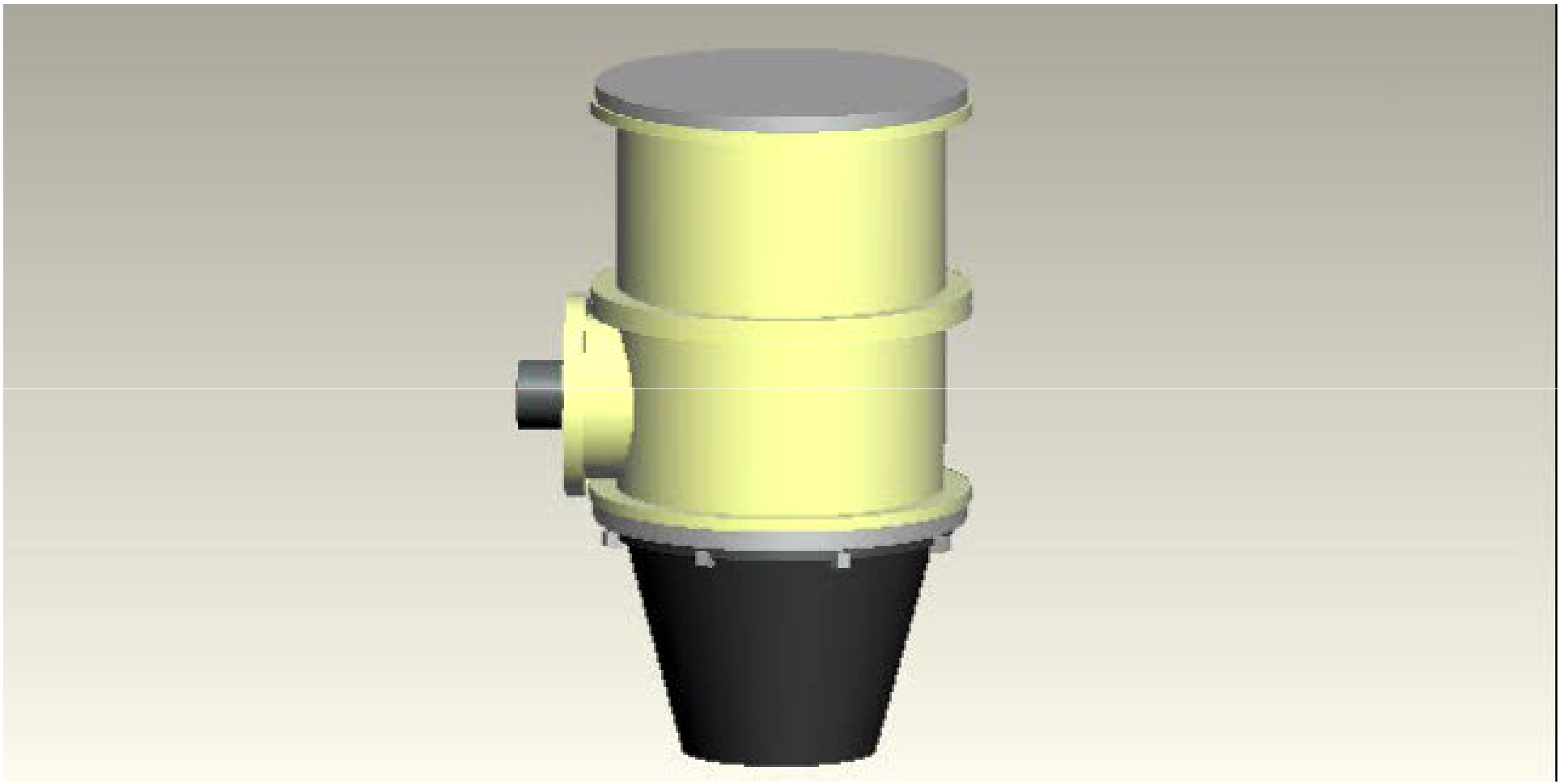

Measurement Procedure

- **Mount 6 inch square samples in sample holder**
- **Pump down to high vacuum (10^{-6} Torr range)**
- Pre sputter to remove surface layer affected by polishing
- Vent and wait for the sample weight to equilibrate (if necessary)
- Initial weight measurement
- **Mount 6 inch square samples in sample holder**
- **Pump down to high vacuum (10^{-6} Torr range)**
- Run ion source and perform QCM differential sputter yield measurements
- Vent and wait for the sample weight to equilibrate (if necessary)
- Weight measurements

Materials and Conditions

- BN is material of primary interest for Hall thrusters from the point of view of erosion and contamination
- Boron Nitride: HBC and HBR grades (GE's Advanced Ceramics), HP grade (Saint-Gobain):
  - HBR, HP - calcium borate is used as binder
  - HBC - no binder
- All three BN grades are hot-pressed graphite-like allotropes of BN. Three grades have similar properties with some differences, e.g. HBR and HP have higher moisture absorption than HBC
- Measurement conditions: Xe ion energies of 60, 80, 100, 200 and 250 eV, incidence angles of 0, 15, 30, and 45 degrees

Sputter Yield Measurement – Weight Loss

Y (mm^3/C):

$$Y = \frac{\Delta m}{\rho \, J_{B,Avg} \, t}$$

where:

Δm = mass change
ρ = density of target material
$J_{B,avg}$ = current of bombarding particles
t = exposure time

Moisture Effects: HBC and HBR

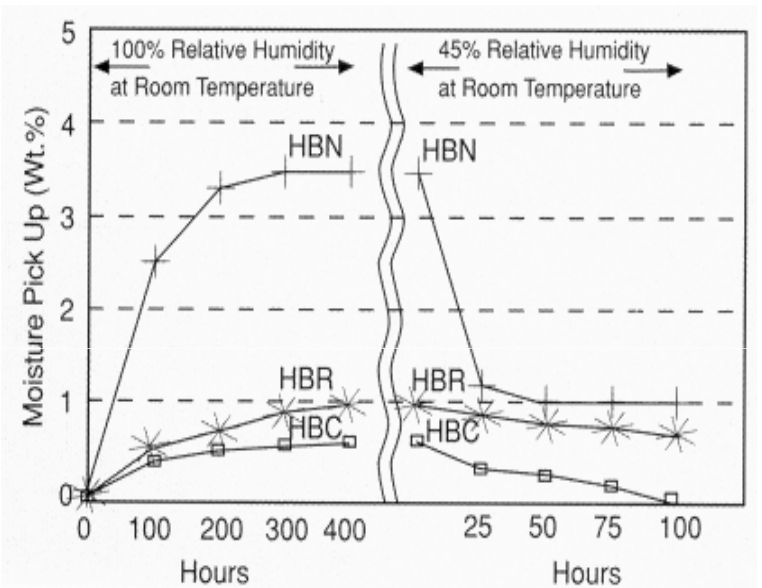

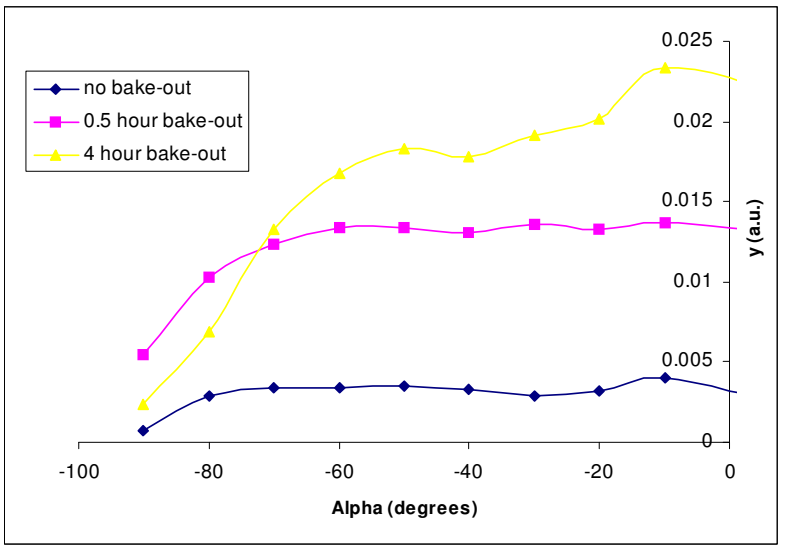

Moisture absorption of various grades of hot-pressed boron nitride (from GE Webpage).
Humidity in the lab is about 40%. It is reasonable to expect that the HBC BN samples will have essentially no moisture pick up, but the HBR samples may have up to 1% pickup.

Moisture Effects: HP

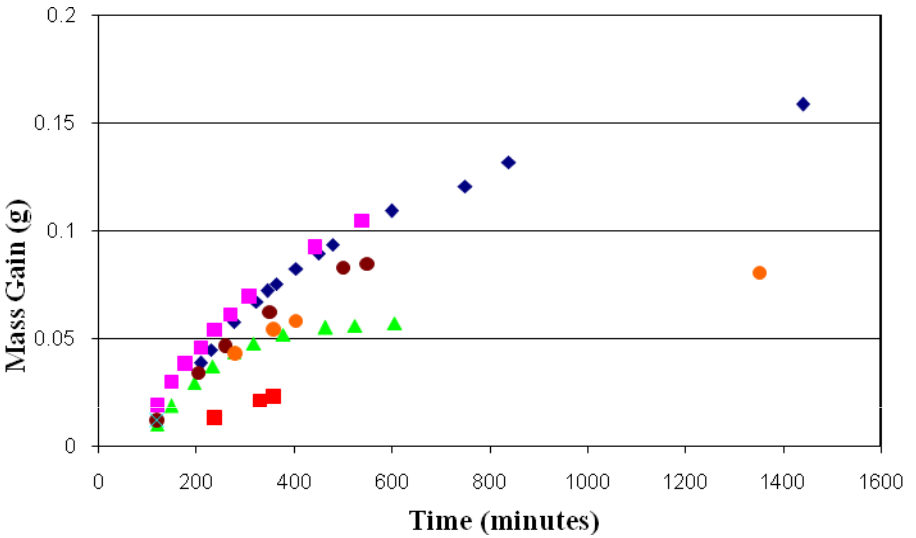

Mass accumulation as a function of time from six different HP BN weighing sessions. Time zero corresponds to 90 minutes after removal from vacuum chamber.

Large mass buildup and variation of individual samples relative to the total before/after mass change of a typical test (~2-10 mg) precludes weight loss measurements of HP BN unless proper measurement procedure is found

Sputter Yield Measurement - QCM

Y ($mm^3/C/sr$):

$$y(\alpha,\phi) = \left[R(\alpha,\phi) {r_{qcm}}^2 \right] \Big/ \left[\rho J_{B,avg} A_s \right]$$

where:

$R(\alpha\phi,)$ = measured mass accumulation rate
ρ = density of target material
$J_{B,avg}$ = ion current incident on the target
r_{qcm} = distance from target center to QCM
A_s = QCM sensor area (0.535 cm^2)

Profile Fitting – Modified Zhang Eqns.

$$y = \frac{Y}{1 - \sqrt{\frac{E^*}{E}}\cos(\beta)} \cdot \frac{\cos(\alpha)}{\pi}\left[1 - \frac{1}{4}\sqrt{\frac{E^*}{E}}\left(\cos(\beta)\gamma(\alpha) + \frac{3}{2}\pi\sin(\beta)\sin(\alpha)\cos(\phi)\right)\right]$$

$$\gamma(\alpha) = \frac{3\sin^2\alpha - 1}{\sin^2\alpha} + \frac{\cos^2\alpha\left(3\sin^2\alpha + 1\right)}{2\sin^3\alpha}\ln\left(\frac{1+\sin\alpha}{1-\sin\alpha}\right)$$

where:

y = differential sputter yield
Y = total sputter yield – FIT PARAMETER
E^* = characteristic energy – FIT PARAMETER

β = incidence angle
α = polar ejection angle
ϕ = azimuthal ejection angle

Sputter Measurement Validation

Total sputter yield for normally incident Xe^+ on Mo

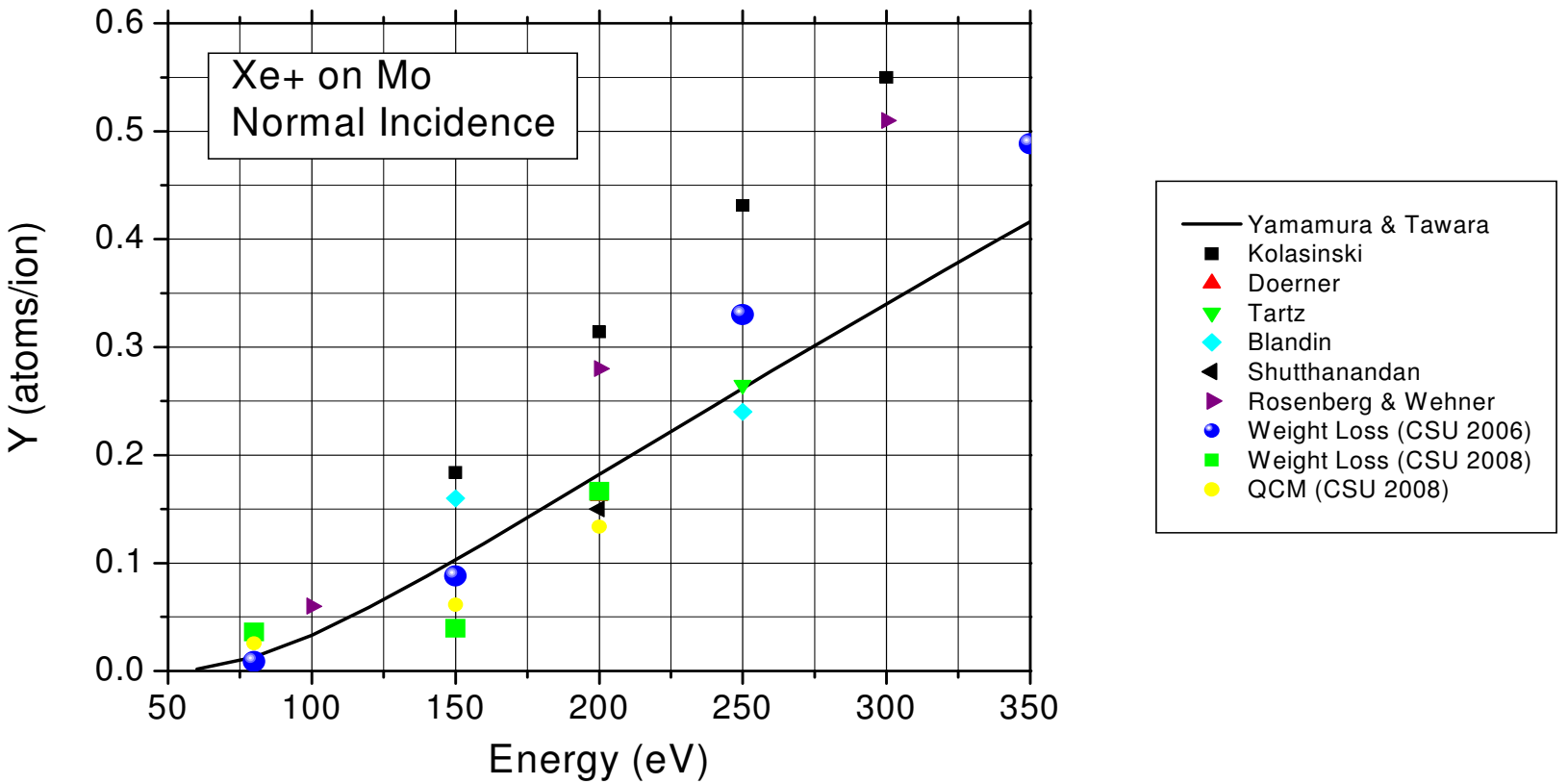

Total Sputter Yield versus Energy (Weight Loss)

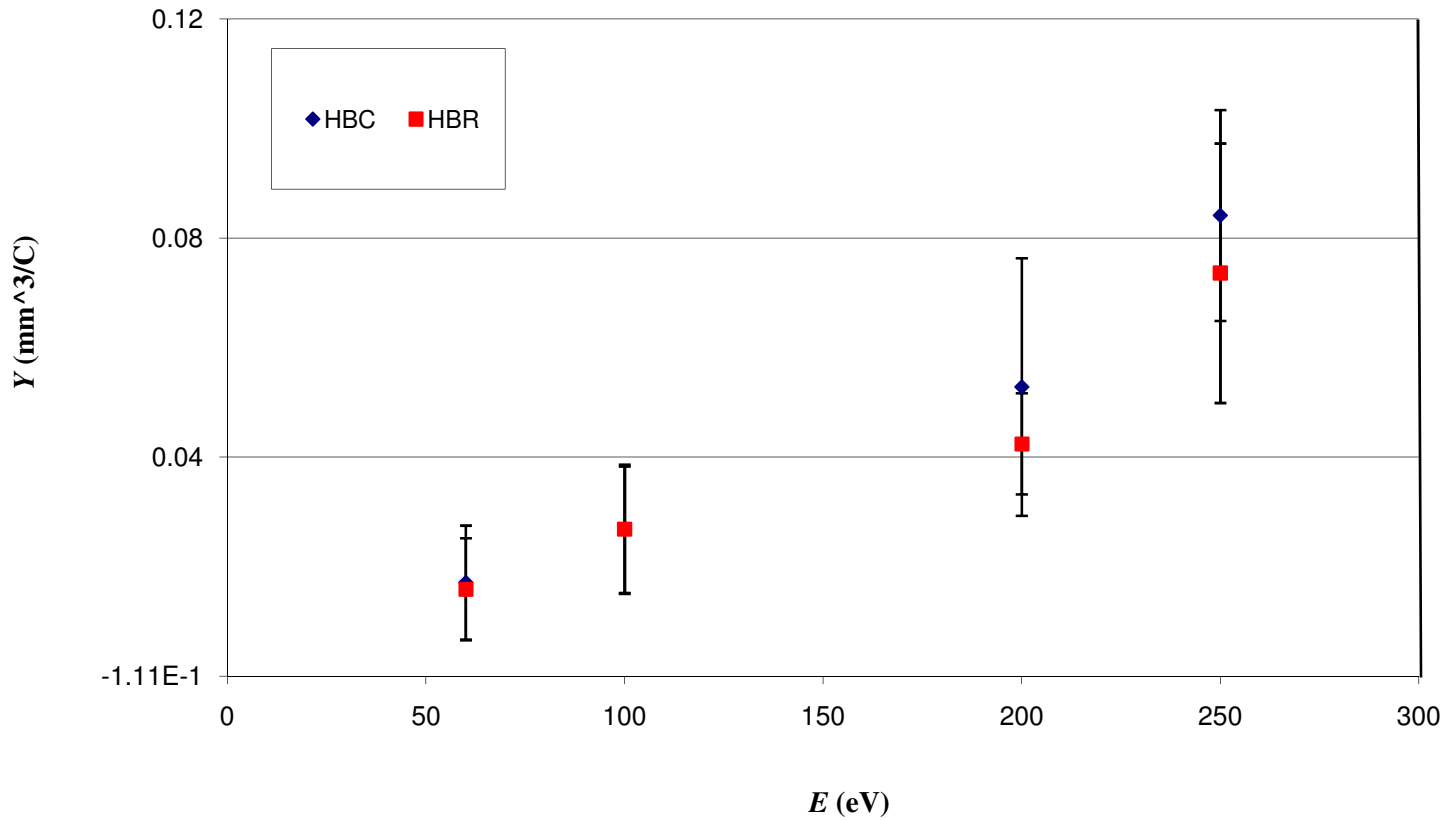

Normal Incidence

Total Sputter Yield versus Energy (QCM)

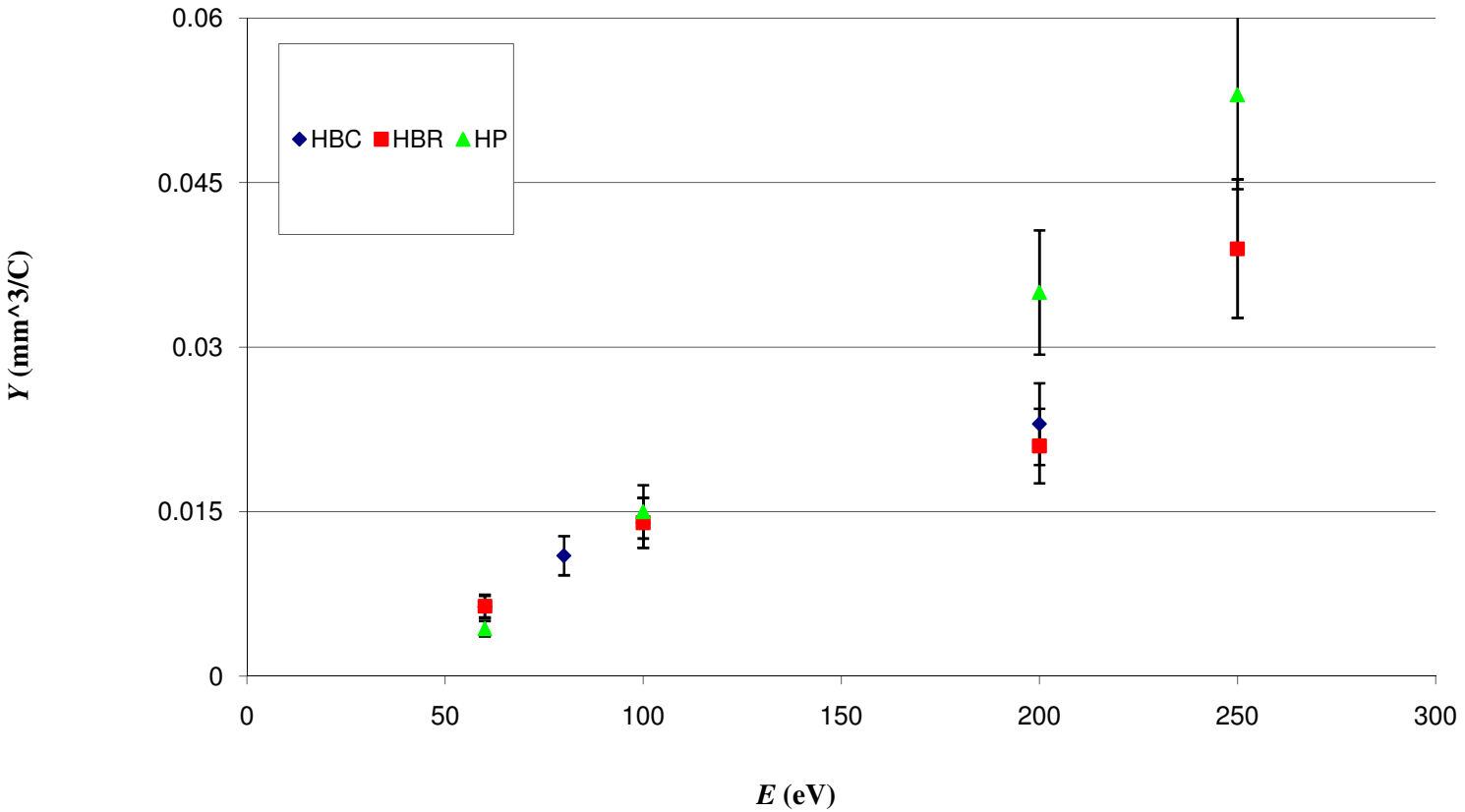

Normal Incidence

Yield $_{\text{Weight Loss}}$ / Yield $_{\text{QCM}}$

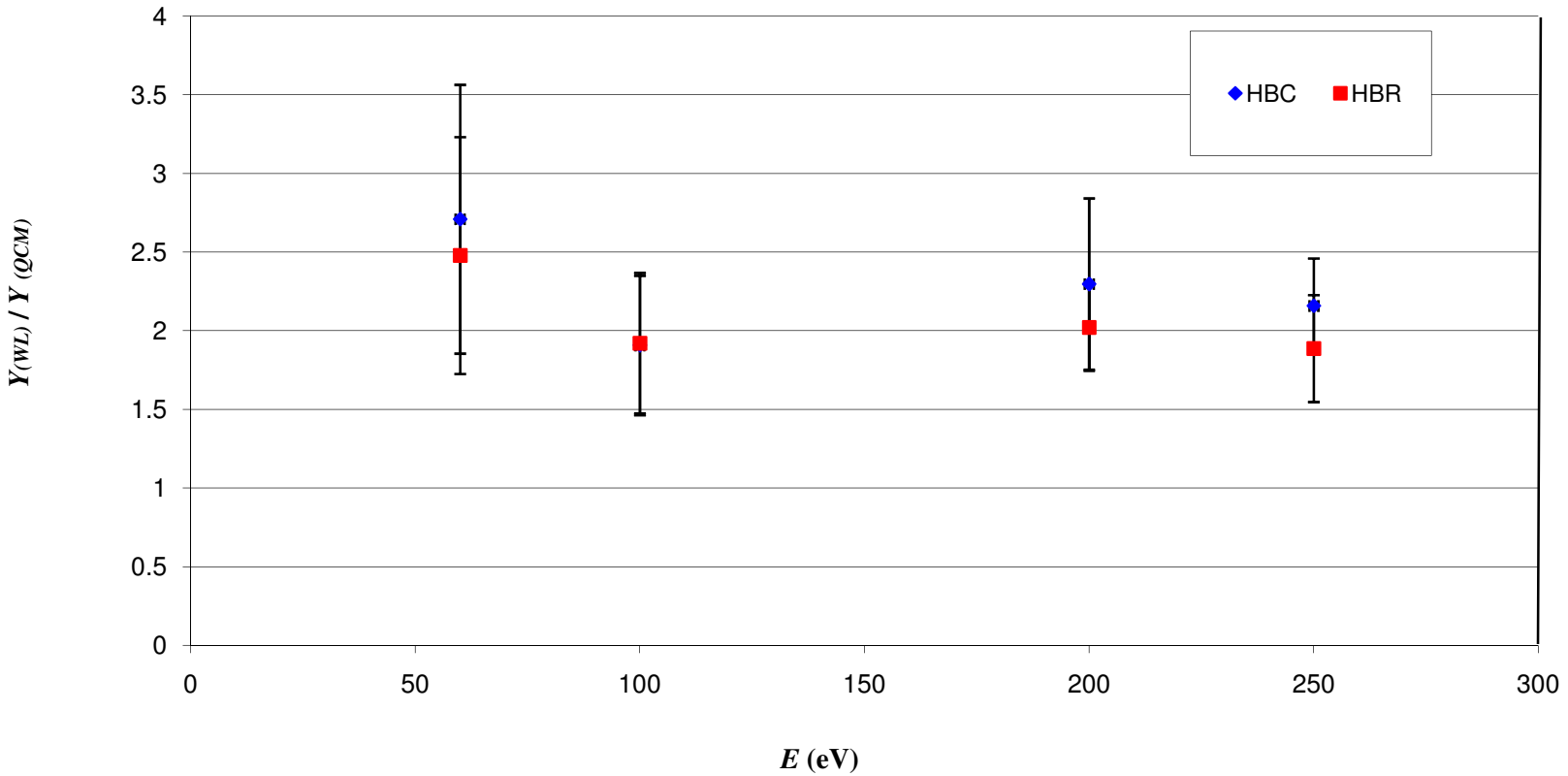

Normal Incidence

$(M_B+M_N)/M_B = 2.30$

M_B - atomic mass of B

M_N - atomic mass of N

Total Sputter Yield versus Angle (Weight Loss)

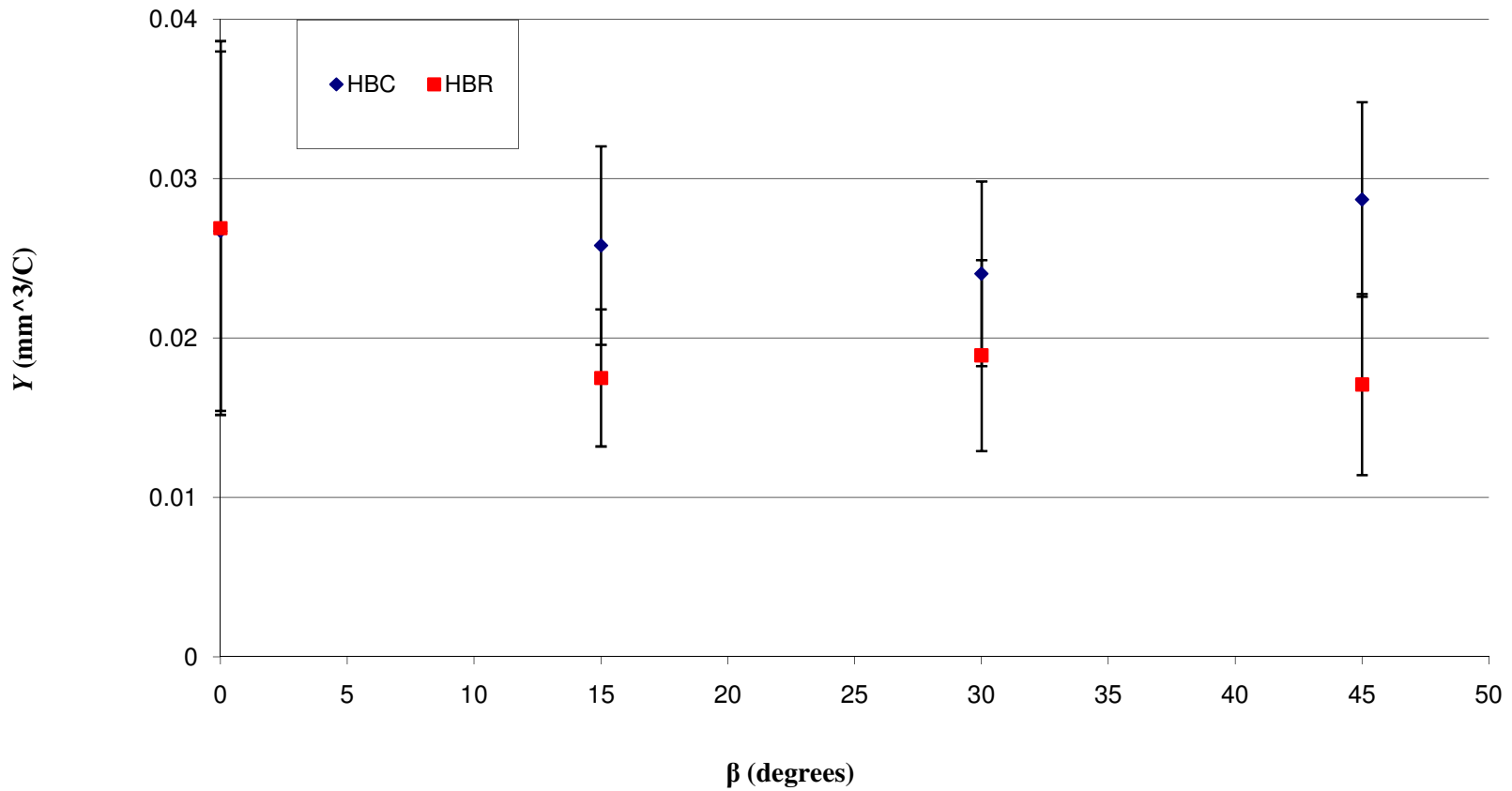

E = 100 eV

Total Sputter Yield versus Angle (QCM)

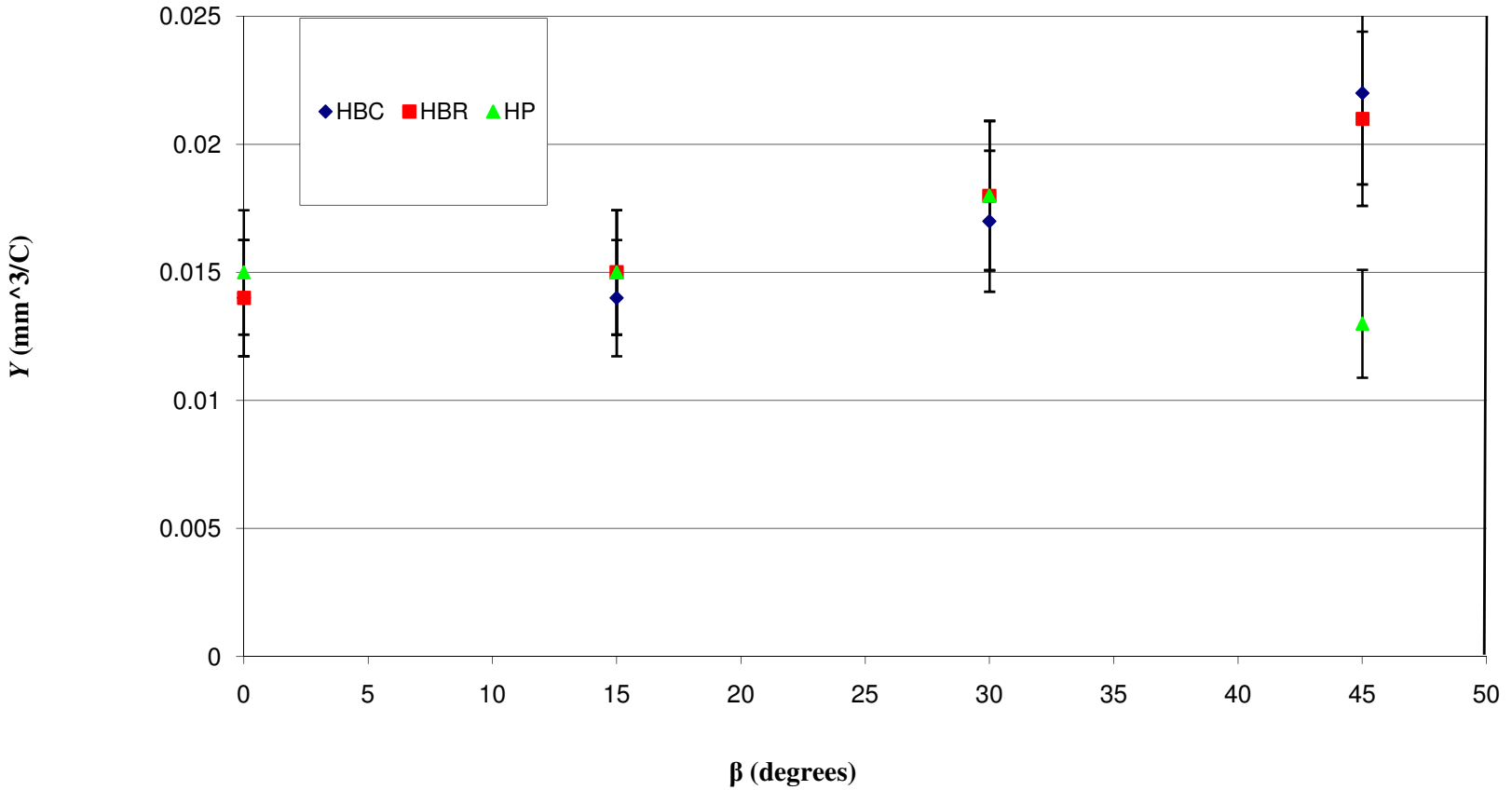

$E = 100$ eV

Comparison with Past Measurements

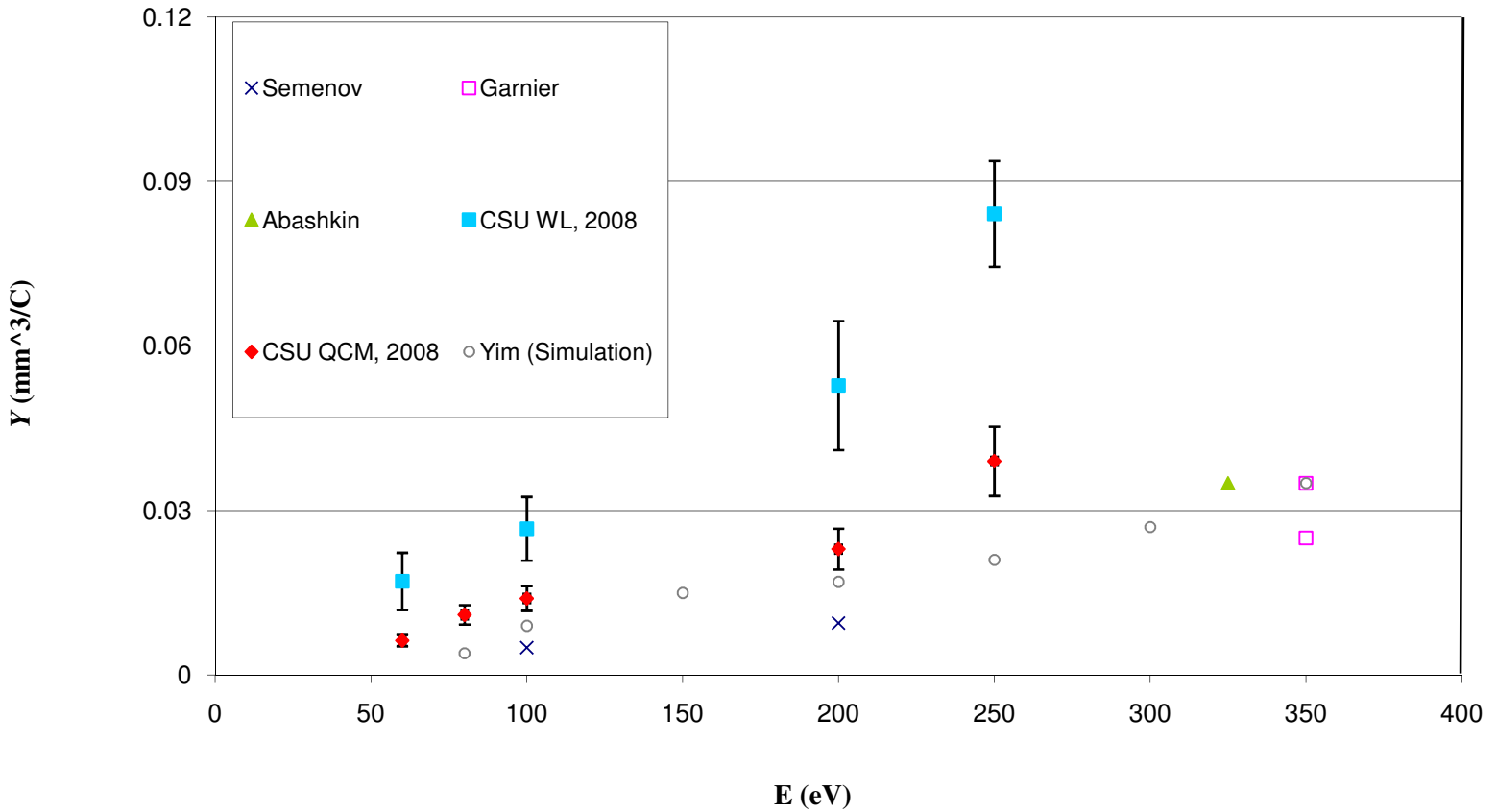

Past measurements limited to minimum of ~100 eV.

Differential Sputter Yield - Xe^+ on HBC BN

$E = 100$ eV, $\beta = 0°$

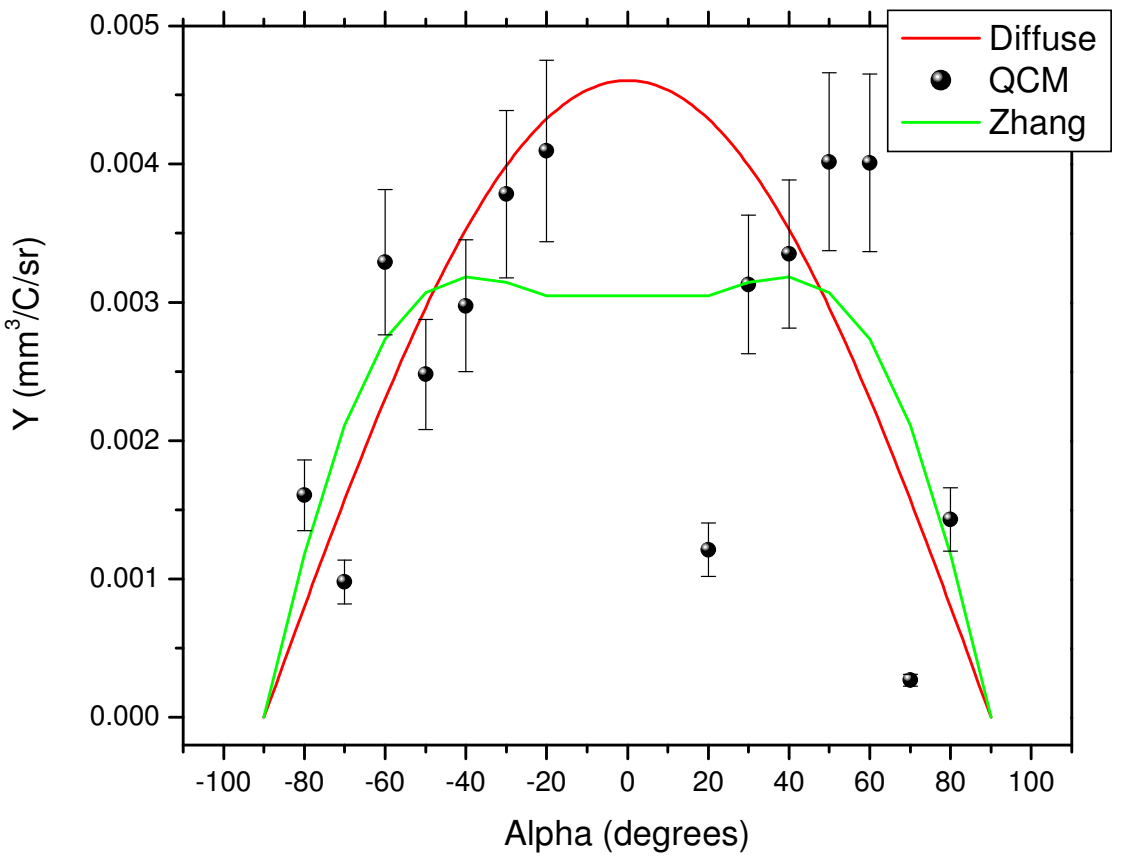

Differential Sputter Yield - Xe^+ on HBC BN

$E = 100$ eV, $\beta = 30°$ (Normal)

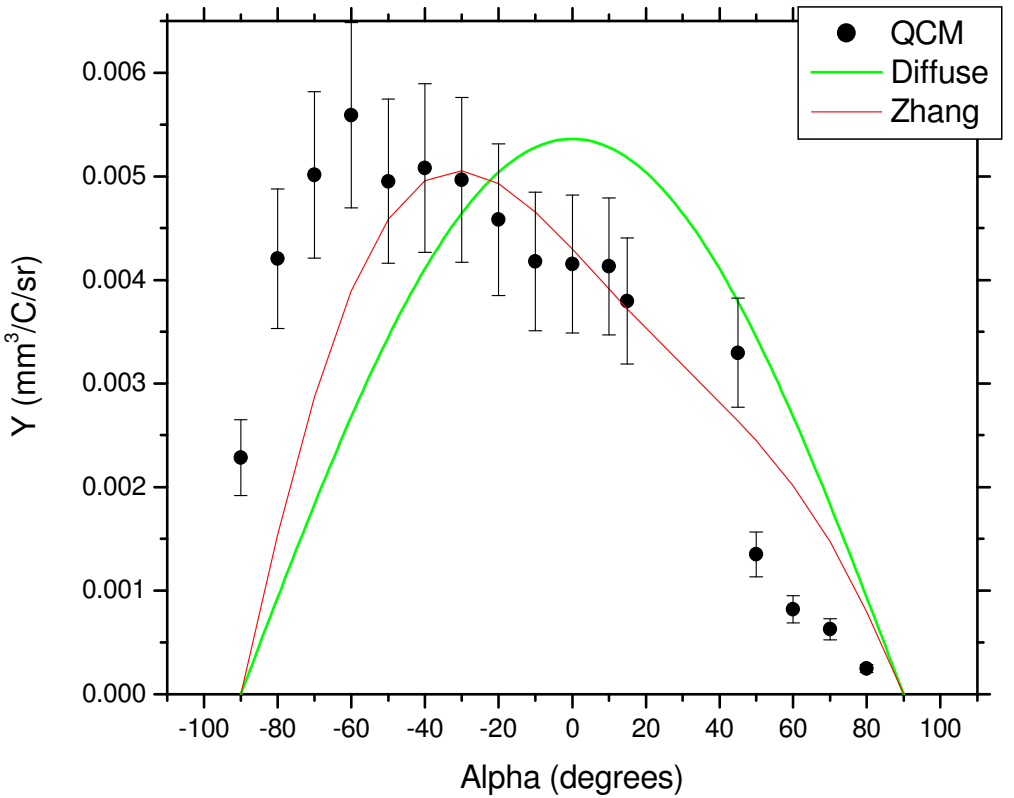

Forward Sputter ⟷ Backward Sputter

Xe^+ on HBC BN – Differential Yield Profiles

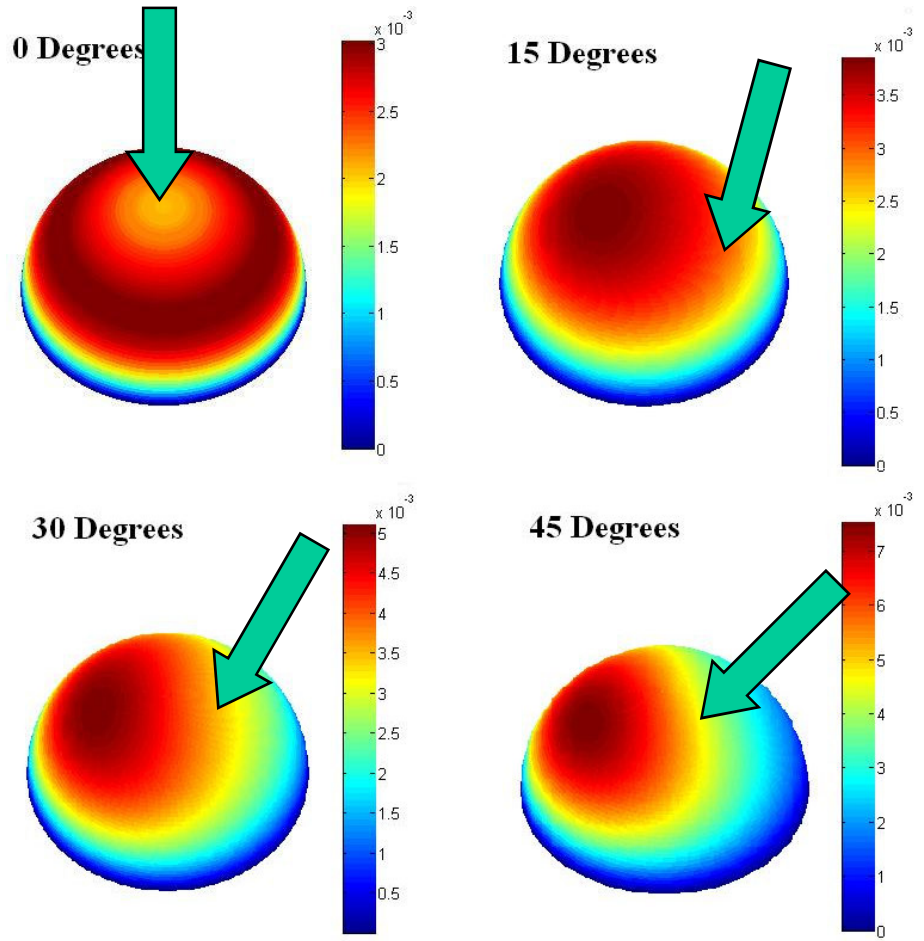

100 eV

Differential Yield Profiles – *E*/E* Shape Parameter

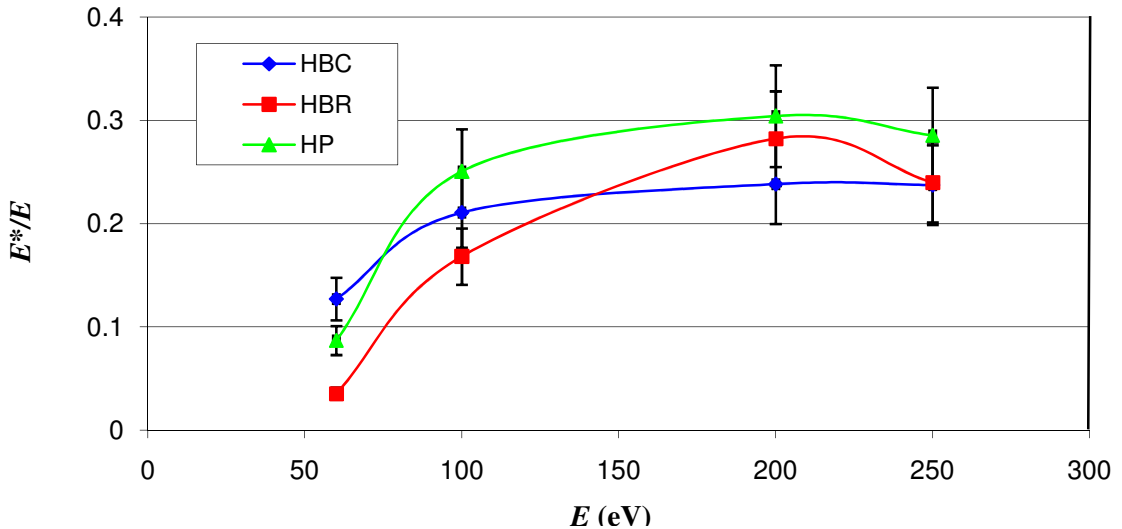

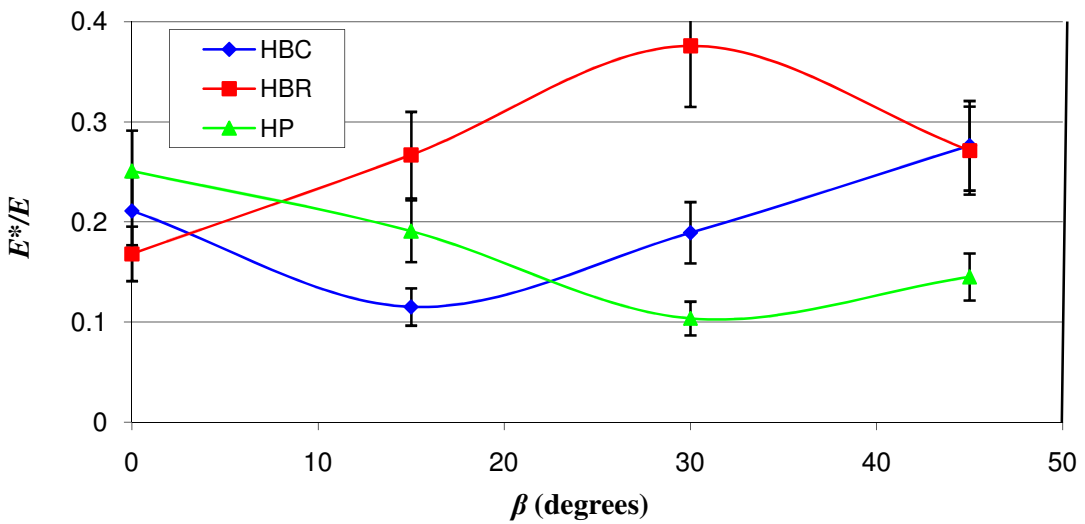

Conclusions

•Use of four-grid ion source with weight-loss and QCM allows sensitive measurement of total and differential sputter yields for different grades of BN at ion energies.

•Total sputter yields for all grades are similar.
•Comparison of weight loss to QCM yields indicates sputtering primarily as atoms.
•Total sputter yields in 100-250 eV range are somewhat higher relative to those in the literature.
•Measurements in the <100 eV range are critical to thruster erosion and reported measurements are amongst the first.

•Differential sputter yield profiles for different grades are relatively similar and show azimuthally symmetric behavior at normal incidence and forward/backward sputtering features at oblique incidence.

Ongoing and Future Work

- Expand test-matrix of energies, angles
- Validation studies (moisture, neutralization effects, Xe ion implantation)
- Improved precision in mass measurement
- Studies of dependence of sputter yields on target temperature

Acknowledgements & Contact Information

•Funding Support:

Air Force Research Laboratory (Edwards Air Force Base, CA)

•Technical Assistance:

Casey Farnell, John Williams, Paul Wilbur (CSU)

•Contact:

Professor Azer Yalin
Dept. Mech. Eng.
Colorado State University
Fort Collins, CO
80523

ayalin@engr.colostate.edu
970-491-8840

Extra Slides

Chamber and Pressures:
•1500 liter/s CTI-8 cryogenic pump
•Chamber base pressure - 5×10^{-7} Torr (after 8-hour bake out)
•Working pressure - 0.6-1×10^{-4} Torr

Ion Source and Beam:
- Typical Xe flowrate - 0.3-0.5 sccm
- Four-grid ion optic system
- Thoriated tungsten hot-filament cathode
- Discharge voltage (V_D) – 30-40 V
- Average current densities ~0.1 mA/cm^2

Sample Preparation:
•Sputter-cleaned for 3-6 hours with a 500-750 eV (~0.2 mA/cm^2) beam

PBN:
•Emission current - 8-20 mA
•Xe mass flow rate = 0.5 sccm
•Voltage bias = -24 V

Azimuthally Symmetric Profiles: $y(\alpha)$

- Simplest case: diffuse (cosine) profile. (Rare, but convenient)
- Over-cosine profiles: high energy ions (all incidence angles)
- Under-cosine profiles: low energy ions (normal incidence)

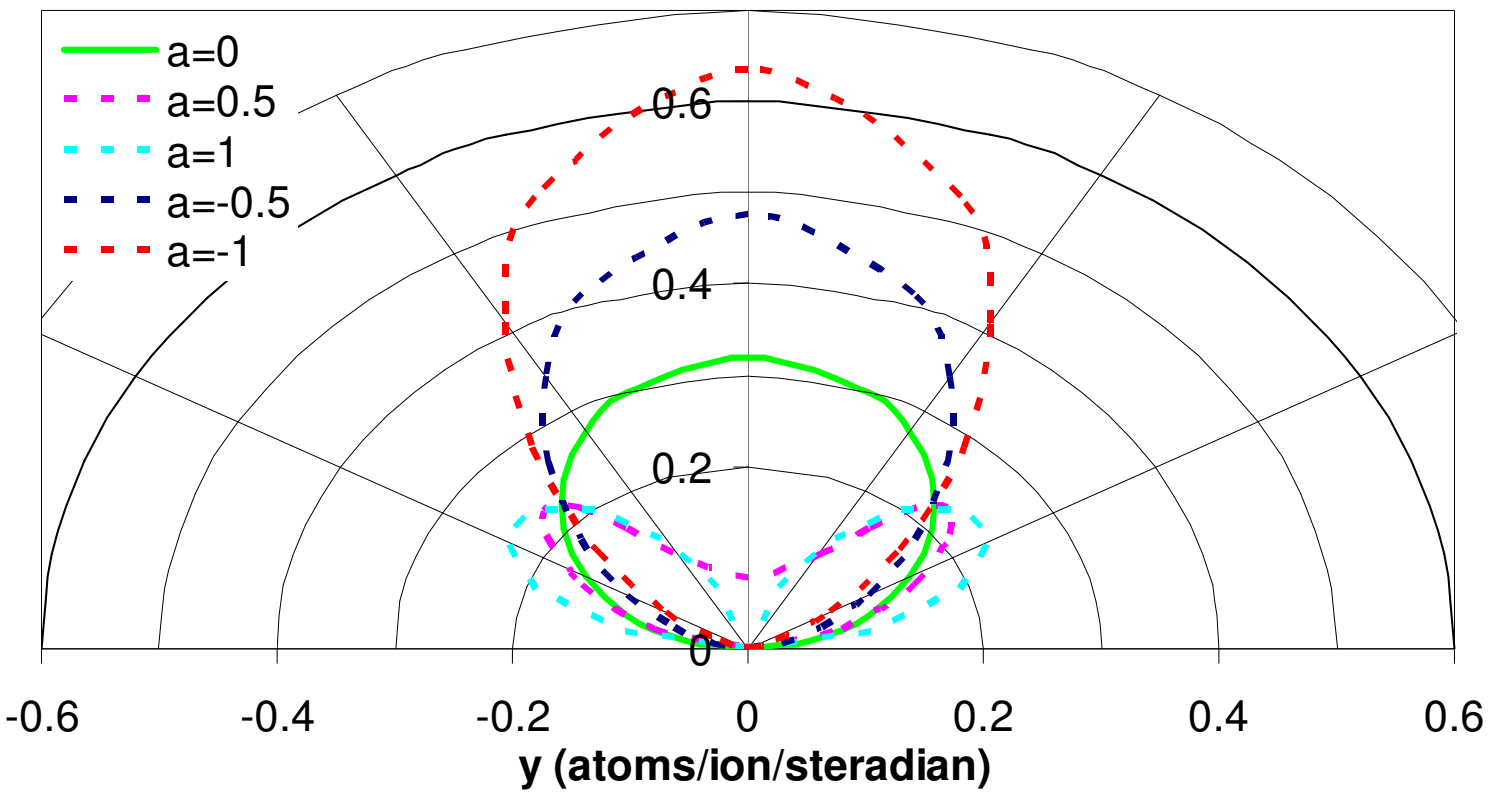

Azimuthally Symmetric Profiles: $y(\alpha)$

350 eV Xe ions normally incident on Mo

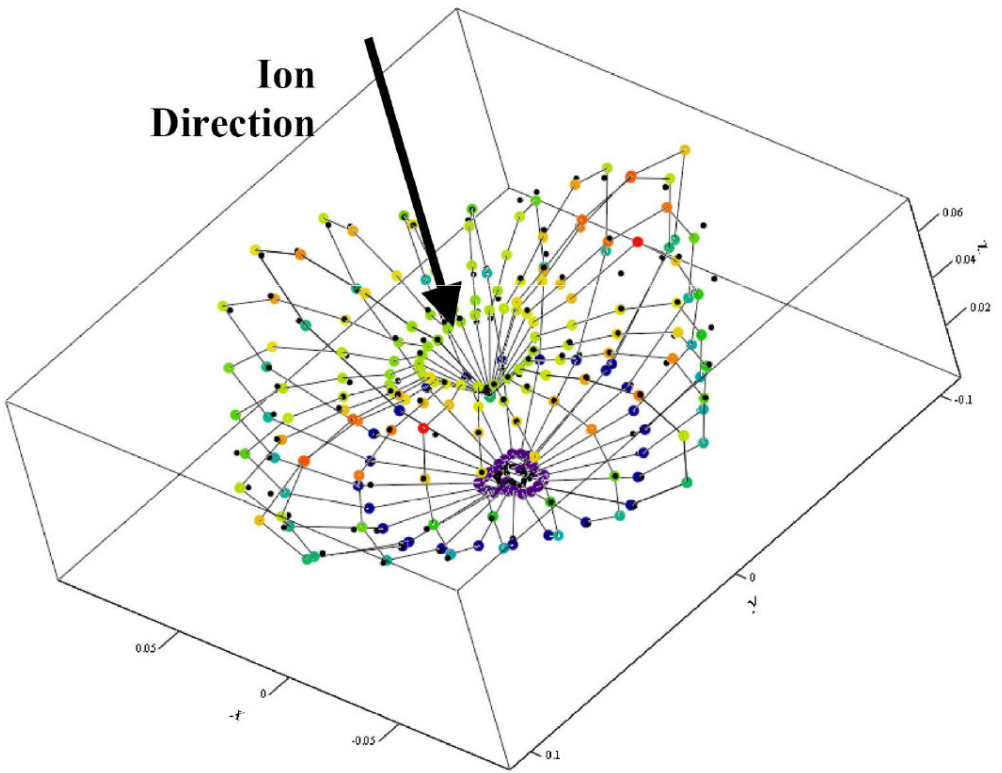

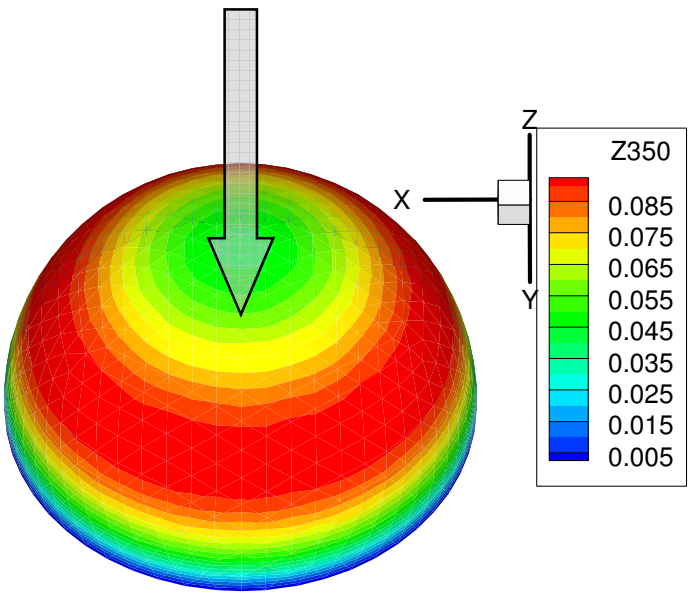

Non-Azimuthally Symmetric Profiles: $y(\alpha,\phi)$

- Anisotropic targets
- **Low energy sputtering** (oblique incidence ions):
  - Isotropic sputtering condition: $(M_iE_r/M_tE_i)^{1/2}<<1$

350 eV Xe ions 30 degree incident on Mo

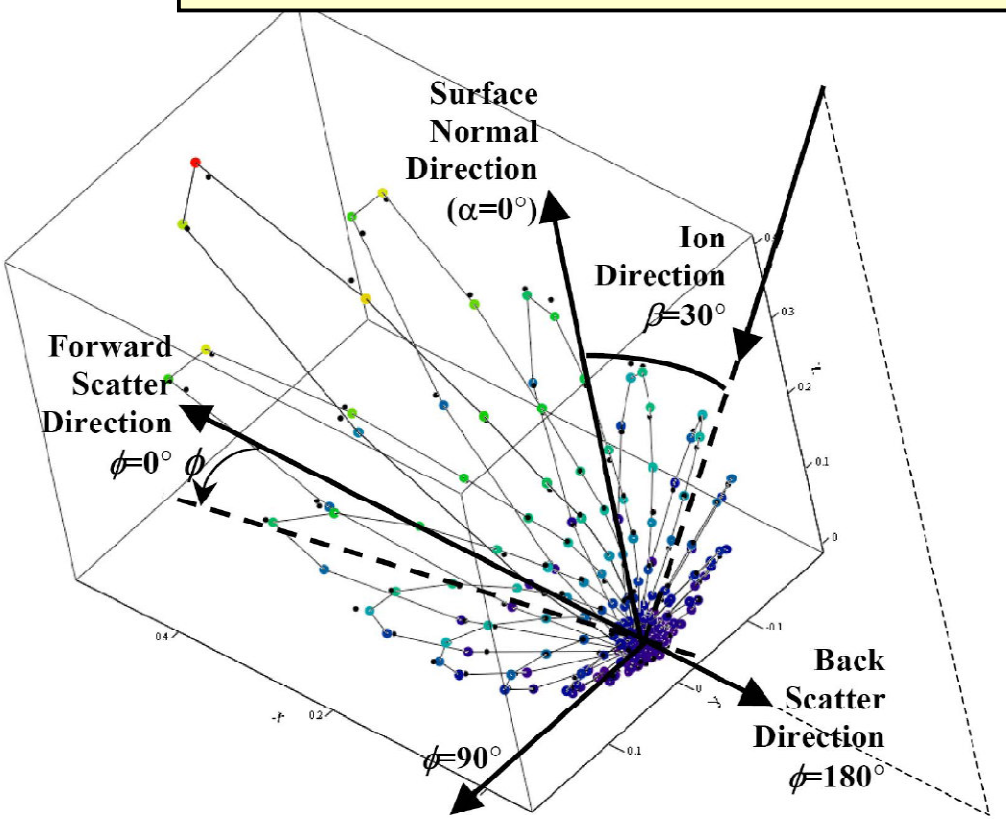

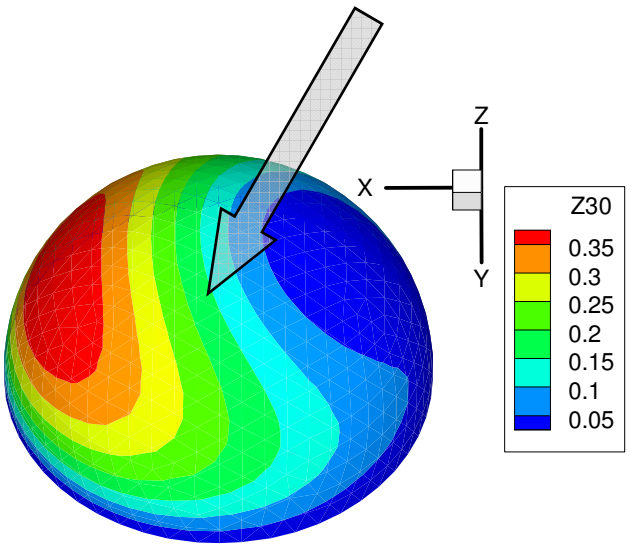

Coliseum Expressions (for reference)

- Constant: $y_C(E,\theta) = C$

- Kannenberg: $y_K(E,\theta) = (C_A + C_B E)(C_P\theta + C_Q\theta^2 + C_R\theta^3)$

- Pencil: $y_P(E,\theta) = C_A E^{0.25}\left(1 - \frac{C_B}{E}\right)^{3.5}$

- Roussel: $y_R(E,\theta) = (C_A + C_B E)(1 - 0.72\theta + 11.72\theta^2 - 3.13\theta^3 - 2.57\theta^4)$

- Yamamura:

$$y_Y(E,\theta) = \left(\cos^{-f}\theta e^{-\Sigma\left(\cos^{-1}\theta - 1\right)}\right) P \frac{s_n(\varepsilon)}{1 + 0.35 U_s s_e(\varepsilon)}\left[1 - \left(\frac{E_{th}}{E}\right)^{0.5}\right]^{2.8}$$

$$f = f_s\left(1 + 2.5\frac{1-\zeta}{\zeta}\right) \qquad \Sigma = f\cos\theta_{opt} \qquad \zeta = 1 - \sqrt{\frac{E_{th,A}}{E}}$$

Total Yield Expressions (Normal Incidence) – Y&T 2/5

- Example of comparison of Y&T expressions to CSU and other data:

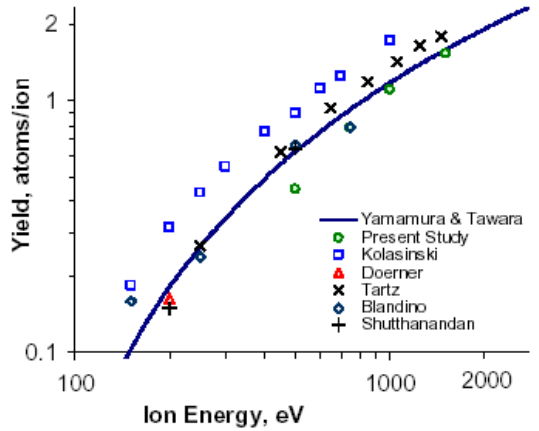

Figure 8. Total yields for Xe^+ on Mo.

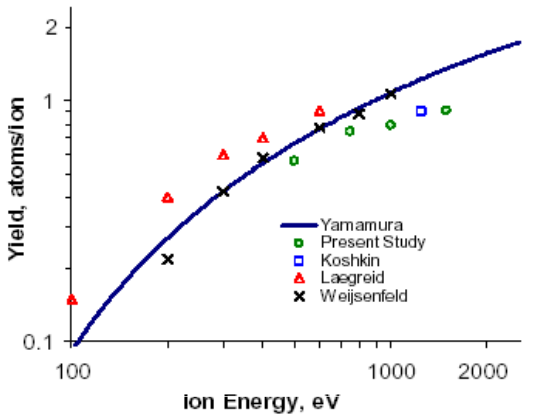

Figure 9. Total yields for Ar^+ on Mo

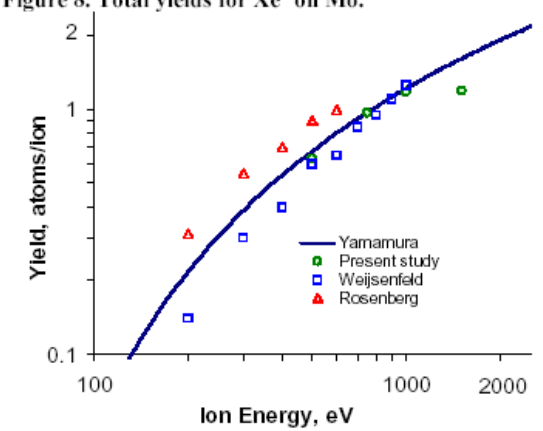

Figure 10. Total yields for Kr^+ on Mo.

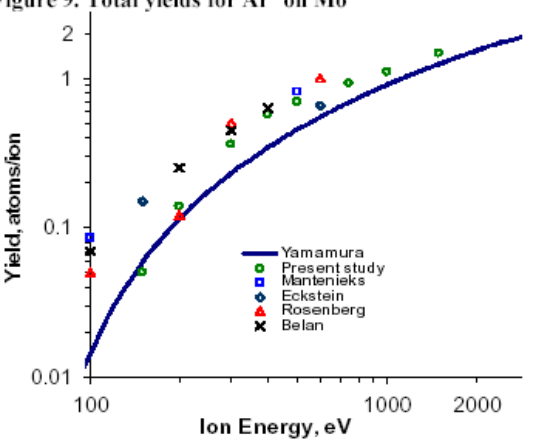

Figure 11. Total yields for Xe^+ on Ta.

From: Differential Sputtering Yields of Refractory Metals by Xenon, Krypton, and Argon Ion Bombardment at Normal and Oblique Incidences, **IEPC-2005-293,** Zoerb et al, Colorado State University

Total Yield Expressions (Varied Incidence)

- Normal incidence total yields $Y(\theta=0)$ can be scaled to give total yields $Y(\theta)$ for varying angle of incidence θ.
- Use approach of Yamamura (as shown on the Coliseum slide). Simple scaling expression is based on tabulated values of "f" and "θ_{opt}".

  See: Y. Yamamura, Y. Itikawa, N. Itoh, "Angular Dependence of Sputtering Yields of Monatomic Solids" IPPJ-AM-26 (1983)
- In this case the database of material constants is relatively limited. For other ion/target materials, the (2) needed parameters can be easily found by fitting CSU (or other) data to these functional forms.
- Expression and example:

$$\frac{Y(\theta)}{Y(0)} := \cos(\theta)^{-f} \cdot e^{-f\cdot\cos(\theta opt)\left(\frac{1}{\cos(\theta)}-1\right)}$$

Example is Ar on Cu at 500 eV (table 3 of paper)

$f := 3.35$ $\quad \theta opt := 49.6$

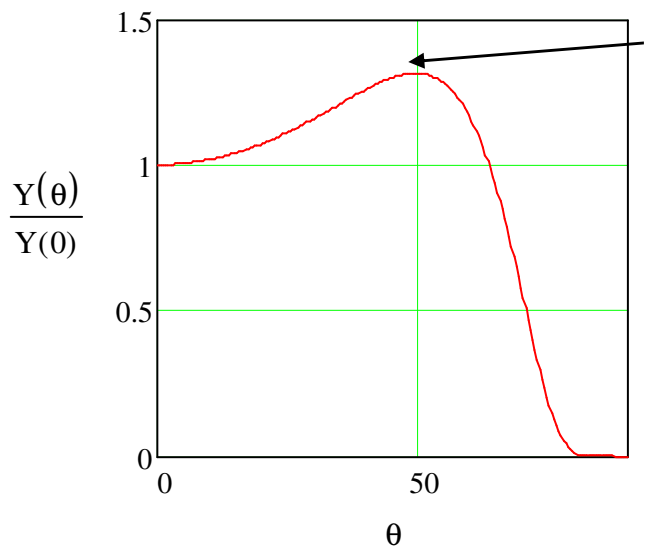

Y peaks at $\theta=\theta_{opt}$ (=49.6° for Ar^+ on Cu at 500 eV).

Differential Sputter Yield Expressions – 3/7

- Base expressions are from:

ANISOTROPIC ANGULAR DISTRIBUTION OF SPUTTERED ATOMS

ZHU LIN ZHANG[a,*] and LAI ZHANG[b]

[a]*Department of Mathematics and Physics and* [b]*Department of Computer Science and Technology, Anhui University of Science and Technology, Huainan, China*

- Differential sputter yield, $y(\alpha,\phi)$:

$$y(\alpha,\phi) = 0.042\frac{\alpha\left(M_2/M_1\right)S_n(E)}{\pi U_s}\cdot\cos(\alpha)\left[1-\frac{1}{4}\sqrt{\frac{E_{th}}{E}}\left(\cos(\beta)\gamma(\alpha)+\frac{3}{2}\pi\sin(\beta)\sin(\alpha)\cos(\phi)\right)\right]$$

where

$$\gamma(\alpha) = \frac{3\sin(\alpha)^2-1}{\sin(\alpha)^2}+\frac{\cos(\alpha)^2\left(3\sin(\alpha)^2+1\right)}{2\sin(\alpha)^3}\ln\left(\frac{1+\sin(\alpha)}{1-\sin(\alpha)}\right)$$

Differential Sputter Yield Expressions – 4/7

Problem 1: Total sputter yields

- The total sputter yields in the Zhang expressions (based on earlier work by Yamamura and others) do not have the flexibility to use free (fit) parameters and do not agree well with data. The total yields are not explicitly included, but can be determined as:

$$Y(E,\beta) = \int_0^{2\pi} \int_0^{\pi/2} y(\alpha,\phi)\sin(\alpha)\,d\alpha\,d\phi = 0.042\,\frac{\alpha\left(M_2/M_1\right)S_n(E)}{U_s}\left[1-\sqrt{\frac{E_{th}}{E}}\cos(\beta)\right]$$

This can be compared with the more complex form of Y&T.

- Example of disagreement of "simple" Zhang total sputter yield with "better" Y&T total sputter yield, computed for Xe^+ on Mo:

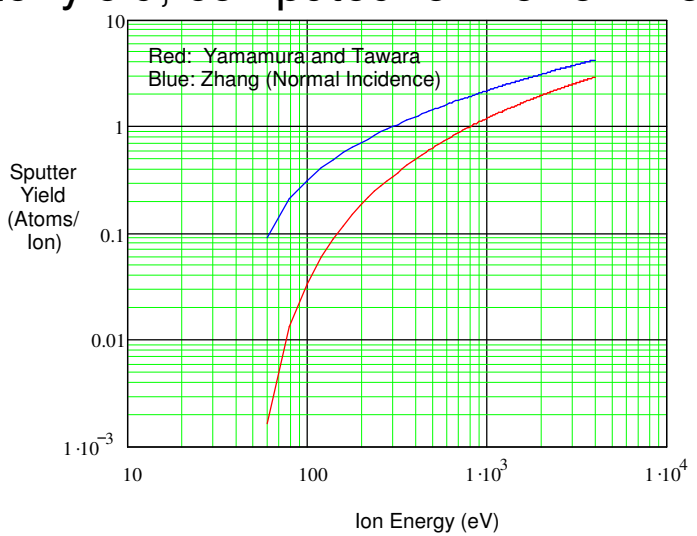

Note: I have used the Y&T value for E_{th} to plot the Zhang total yield. Zhang suggests fitting his curve to data to obtain values of E_{th}, but (at least in this case) such an approach also does not allow good agreement with the Y&T yields (which do agree well with measurement).

Differential Sputter Yield Expressions – 6/7

Problem 2 – Threshold Energy

- Comparison of experimental differential sputter yield profiles with those calculated from Zhang expressions using "*a priori*" E_{th} values (from Y&T) does not give good agreement.
- Example: Xe^+ on Mo, 45° incidence, 750 eV

Experimental (Polar) Surface

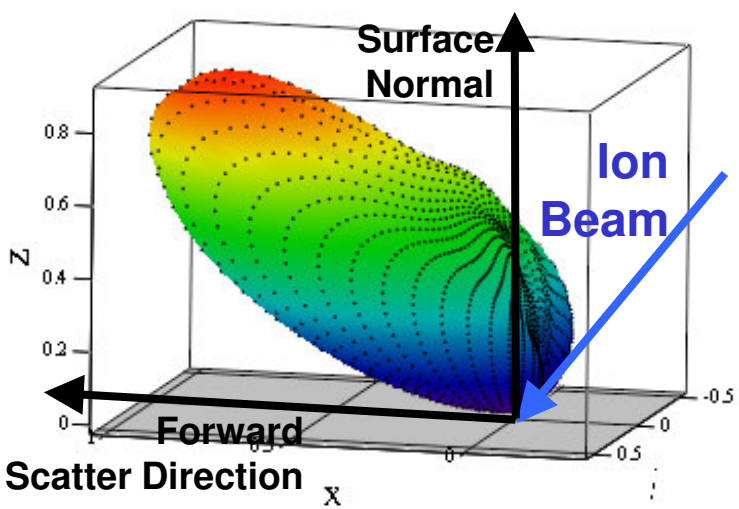

Zhang (Polar) Surface using "*a priori*" E_{th} =46.83 eV

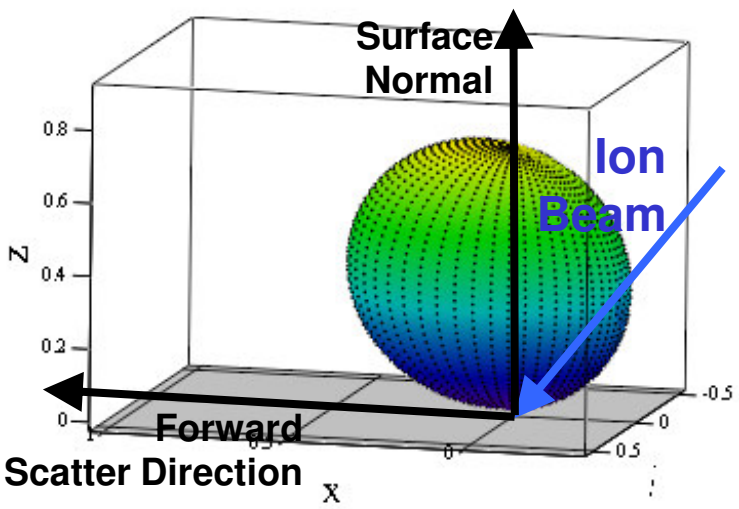

Notes:

1. Experimental surface from CSU Quartz Crystal Microbalance Data (see AIAA 4336-2006).
2. Surfaces are plotted with same scales and correspond to same total yield (total yield is not ∝ volume).
3. Zhang surface is too "diffuse" owing to large E/Eth ratio (see next slide).

Differential Sputter Yield Expressions – 7/7

Solution of Problem 2 – Fit experimental profiles to find *E** values

- Improved agreement between measured angular profiles and the Zhang expressions can be found by using "fitted" values of *E** in place of E_{th}. (We do a least squares fit to find value of E* giving best agreement between experimental profile and $y(Y,E,E^*,\beta,\alpha,\phi)$. For a given ion target combination we find that E* varies with ion energy (likely due to surface texturing effects, possible variation of binding energy with incident ion energy etc.)

Experimental (Polar) Surface

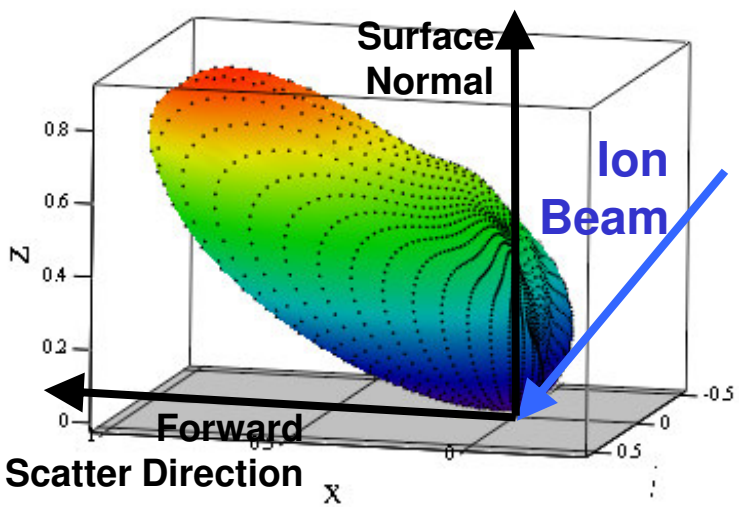

Zhang (Polar) Surface using fitted E* = 390 eV

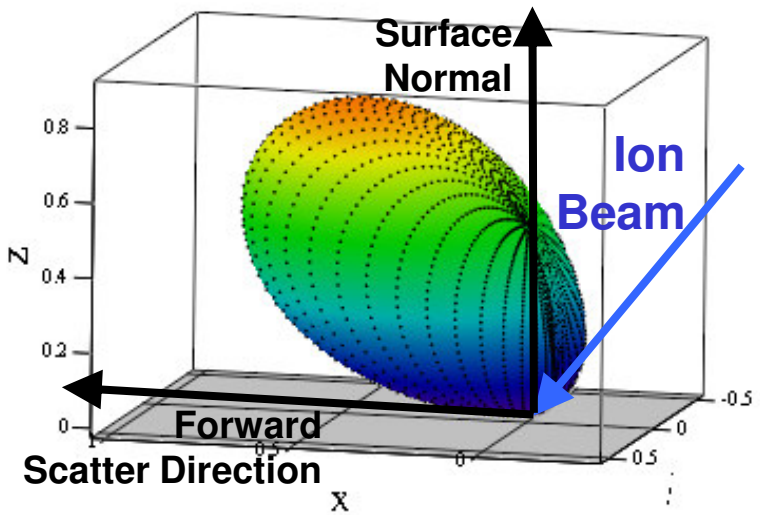

Notes:

1. Zhang surface with E* better captures forward scatter (non-diffuse) behavior (though is still slightly too diffuse, see AIAA 4336-2006). For cases studied, agreement between profiles improves to <std><~15%.
2. Both surfaces are plotted with same scales and correspond to same total yield.